Exploring Aquifer Sustainability

Monitoring Groundwater Wells through Decentralised Measurements and Modelling: a Case Study of Kumasi, Ghana

CEGM3000: Multidisciplinary Project

I. Backers, T. Graafland, E. Kalitsounakis, L. Reichel, Z. Wang

TU Delft

KNUST
KWAME NKRUMAH UNIVERSITY OF SCIENCE AND TECHNOLOGY

Exploring Aquifer Sustainability

Monitoring Groundwater Wells through Decentralised Measurements and Modelling: a Case Study of Kumasi, Ghana

by

I. Backers, T. Graafland, E. Kalitsounakis, L. Reichel, Z. Wang

Student Name	Student Number
Irene Backers	4960947
Tara Graafland	5145503
Evangelos Kalitsounakis	6052649
Lilian Reichel	5999049
Zeyu Wang	5911095

Supervisors:	Dr. E. Abraham
	Dr. Ir. I. Monney
	Dr. G. Rongier
	Ir. P. Amihere-Ackah
	Ir. G. Wiersma
	Ir. F.E. Riakhi
Project Duration:	September, 2024 - November, 2024
Faculty:	Faculty of Civil Engineering and Geosciences, Delft

Style: TU Delft Report Style, with modifications by Daan Zwaneveld

TU Delft

KNUST
KWAME NKRUMAH UNIVERSITY OF SCIENCE AND TECHNOLOGY

Acknowledgements

First and foremost, we would like to thank our primary supervisor, Dr. E. Abraham for his continuous support and guidance throughout the project. His input has shaped this project to the report we can proudly present today. Equally, Prof. I. Monney has helped us immensely during our time in Kumasi in terms of formulating our research and obtaining different types of data. Dr. G. Rongier and Ir. F.E. Riakhi have supported us with processing the modelling data, which we are extremely grateful for. Further thanks are in order for Ir. G.C.M. Wiersma, who counselled us in formulating and preparing the research in advance.

Many others have helped us along the way, including but not limited to Prof. N.C. van de Giesen, Dr. F.O. Annor, Clement Okyere Darko, McCarthy Agyapong, GLS drilling company, and the property owners of the wells used in this project. We are grateful for their kindness and help, which made this project as it stands today.

A special thanks to our daily supervisor Paul Amihere-Ackah, who has supported us along every step of the project and made a lot what was done in this research possible. We sincerely hope this research will help him with his own research in turn, and we wish him all the best in his future career.

To all, thank you.

Abstract

Due to quick population growth and urbanisation in Kumasi, Ghana, groundwater depletion is accelerating, and land cover changes reduce the rate of natural infiltration. A promising measure to combat rapid aquifer depletion is implementing Managed Aquifer Recharge (MAR), by rooftop rainwater harvesting and pumping this into wells. The objective of this paper is to delineate the (qualitative) impact of precipitation through Managed Aquifer Recharge on the groundwater level, by analyzing groundwater level changes of sites with and without MAR around Kumasi. To achieve this, multiple groundwater level and flow models have been constructed over different time periods with varying temporal resolutions to show the short- and long-term effect of precipitation on the groundwater level on sites with and without MAR. A rapid increase of groundwater level is observed during rain events, followed by a decelerating curve of infiltration towards areas with lower elevations. This dissipation is much faster in areas with high hydraulic conductivity (hours) than with low hydraulic conductivity (weeks). The groundwater level is recharged by MAR less in the dry season than in the wet seasons. MAR has a highly positive influence on the groundwater recharge. It will be most crucial to implement MAR in high elevations, where the overburden has low hydraulic conductivity, as natural recharge is limited here. The lack of soil and hydraulic head data limited the reliability of the models. Therefore, it is recommended to extend the database in these and additional research areas, aiming to differentiate the effect of MAR and the natural infiltration on the hydraulic head level.

Key words: Managed Aquifer Recharge (MAR), groundwater level, precipitation, aquifer depletion, rooftop rainwater harvesting, hydraulic conductivity, Kumasi, Ghana.

Contents

1

Introduction

1.1. Project Description

Groundwater has been a safe and reliable source of drinking water in large parts of the world, as it can take up and retain vast amounts of naturally filtered water over long periods of time. Nevertheless, around half of the global population suffers from water scarcity part of the year [59] and for at least three billion people the quality and quantity of the water they depend on is unknown due to lack of monitoring [61]. Rapid population growth combined with the effects of climate change mean that groundwater sources are expected to deplete faster, posing a threat to water availability in already challenged areas.

The city of Kumasi in Ghana is such an example. For the past decades, groundwater extraction has grown to exceed the recharge of the groundwater aquifer; the natural recharge decreases because of more impenetrable surfaces such as asphalt or roofs, while more groundwater is extracted due to higher water demands. The groundwater aquifer is not well monitored, resulting in large uncertainties about the amount of stored groundwater and the estimated groundwater recharge in the rain season. As part of the African Water Corridor (AWC) initiative, this project aims to improve the monitoring of groundwater in Kumasi to ensure sustainable groundwater use for future generations and thereby contribute to the UN sustainable development goals number six: ”Clean Water and Sanitation” and twelve: ”Responsible Consumption and Production” [61]. The AWC’s primary goal is to ensure that a lack of (drinking) water is not a limiting factor for humanitarian and ecological growth in Africa.

Out of great concern over groundwater depletion in Kumasi, there is a need to raise awareness about groundwater challenges, promote sustainable use and encourage artificial groundwater recharge. Managed Aquifer Recharge (MAR) is a promising way to limit groundwater depletion and ensure prolonged storage of rainwater that can be used during dry seasons. One simple type of MAR system has been employed as a pilot project in a peri-urban area of Kumasi since June 2023; By collecting rainwater from the rooftops of 4 houses and injecting it directly into the adjacent open wells, more rainwater, which would otherwise become surface runoff, is able to infiltrate to recharge the groundwater. To measure the hourly groundwater levels in the wells containing the MAR systems and provide us with a data record of over a year vanEssen divers are set.

As the hydraulic head data from the wells in the pilot site are biased by the influence of MAR, differentiating the contribution of natural recharge and the contribution of MAR is extremely difficult. This can be tackled in hydro-geological modelling in two different ways. One can assume all changes in water levels are a result from injection through the wells, where natural infiltration is disregarded. The other, which this report focuses on, assumes that changes in hydraulic head are the result of the combined effects of natural infiltration and changes in the saturated zone. This implies that the total changes observed in the wells, including those partially attributed to MAR, are present throughout the entire model area.

To gain more insight on how to differentiate the influence of natural recharge and MAR, we have installed three divers at a different site that does not utilize MAR to monitor groundwater levels. In addition, soil

samples of a shallow borehole have been analyzed to determine the subsurface properties in one of the two areas. Together, these data provide the basis for an overburden aquifer groundwater flow model, to determine the relation between groundwater flow and precipitation over time. This leads us to the following research objective.

1.2. Research Objective

Delineating the (qualitative) impact of precipitation through Managed Aquifer Recharge on the groundwater level, by analyzing groundwater level changes of sites with and without MAR around Kumasi, Ghana.

To fully achieve this objective, it is essential to:

- Find the relation between groundwater level fluctuations and precipitation;
- Find the volumetric difference in groundwater between the study area with and without MAR;
- Estimate the amount of rooftop area and wells that need to be connected to a MAR system to avoid further groundwater depletion in the Kumasi peri-urban area.

1.3. Report Structure

First and foremost, the background of the research area is investigated with relation to groundwater in chapter 2. As part of this, it is important to understand precipitation patterns, human influence, and the underlying aquifer properties. The concept of MAR will be introduced in more detail as well. Secondly, the available data is described in chapter 3, together with a detailed description of all methods used to address all aspects of the research objective. Following, the results of the analysis will be presented in chapter 4, connecting their interpretations to answer our research objective. Though the focus will lie on a specific type of model to incorporate MAR, a different type of model is discussed in chapter 5. In chapter 6 we discuss the uncertainties and limitations that remain as a challenge and quantify their impact on our model outcomes. Chapter 7 and 8 will give our main conclusions on the research objective with respect to the overlying challenge of groundwater depletion and our recommendations for future research that should be done in order to achieve sustainable groundwater use in Kumasi.

2

Background Information

2.1. Area of Research

Once named the “Garden city of West Africa” by Queen Elizabeth in 1940 for all its greenery and trees [15], the Kumasi Metropolitan Area (KMA) is now home to almost 4 million inhabitants (2024) [60]. When including the peri-urban area, the city stretches over 254 km^2 [16] and is estimated to house 10 million people.

As the largest city of Ghana and capital of the Ashanti Region, Kumasi is located in the rainforest region near Lake Bosomtwe at an elevation of 250-300 meter. The city was founded by Asantehene Osei Kofi Tutu I around 1680 [17]. The location and name of the city arises from the story about Okomfo Anakye. It is said that Okomfo Anakye, priest of the Ashanti Empire planted two Kum seeds, one in Kwaman and the second in Kumawu. One of the seed became a big tree, the other seed died. The location where the tree grew was chosen by Osei Kofi Tutu to become the capital of his empire and is now known as Kumasi. The name Kumasi means ‘under the kum tree‘ and originates from the Twi word ‘kumase’, where ‘kum’ refers to the tree and ‘ase’ means under (I. Monney, personal communication, September 4, 2024).

According to the UN World Population Review it is expected that the metropolis will keep growing to 5.3 million inhabitants by 2035 with a growth rate decreasing from 3.59% in 2023/24 to 2.56% in 2034/35 [68]. This rapid urbanisation comes with the paving of once green areas, which has direct consequences for the natural infiltration of rainwater [57].

2.1.1. Climatology of Kumasi

Kumasi, Ghana is located in West Africa just north of the equator at latitude 6.7, longitude -1.6 with the Gulf of Guinea South of Ghana and the Sahara desert in the north as can be seen in Figure 2.1. According to the Köppen climate classification, Ghana has a tropical savanna climate with a dry winter (Aw-classification). Due to its proximity to the equator, Kumasi knows two seasons, a dry and wet season. Moreover, temperatures and daylight hours are fairly constant throughout the year, with the average daily maximum temperature being 31.3°C [63] and the daylight hours varying from 12 hours 31 min on the longest day to 11 hour 44 min on the shortest day [64].

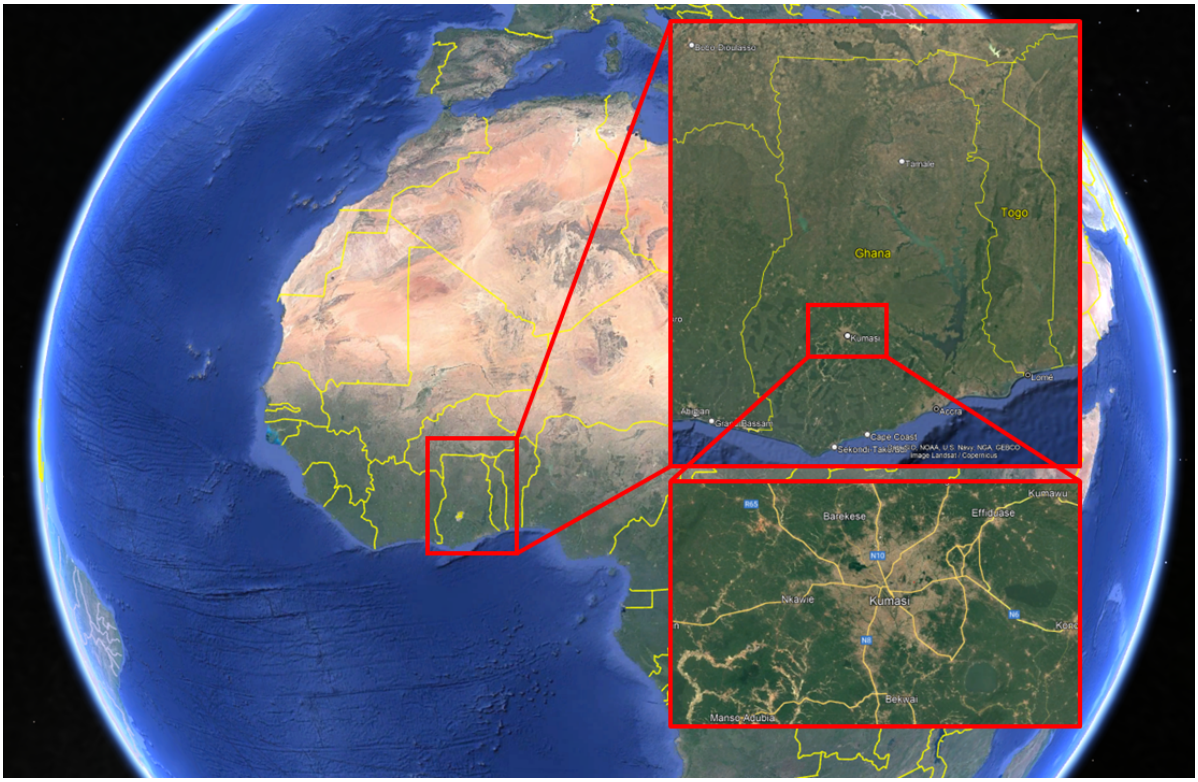

Figure 2.1: Location of Ghana and Kumasi from Google Earth Map [30].

The highest temperatures are reached during the dry period that starts in November and lasts till February. The dry season, or Harmattan, occurs in the months with the lowest sun. These months are characterized by a northeasterly trade wind, equally named Harmattan, that blows dry and dusty air from the Sahara over West Africa towards the Gulf of Guinea [52]. The wet season lasts from March until October and is characterized by southwesterly West African monsoons blowing over the Atlantic ocean and bringing slightly cooler, moist air and rain [53]. The rain season can be split in a major rain season from March to July and a minor rain season in September and October with a slightly dryer month in August.

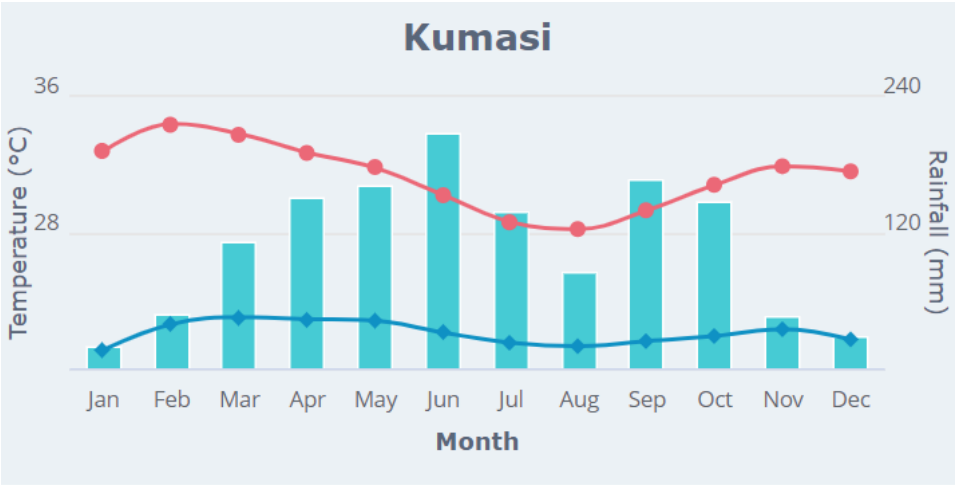

Figure 2.2: Climate in Kumasi, average temperature and rainfall per month for the climatological 30-year period 1981-2010 [67].

2.1.2. Urbanisation in the Kumasi Metropolis

Urbanisation is formulated by B.F. Frimpong as “the development of urban/built-up areas for the provision of houses, industries, and other infrastructure, such as transportation networks and other social amenities that support the existence of humans” [26]. The UN Population Division expects that the world’s urban population will increase by more than two thirds by 2050. Of this increase, 90% will be in the cities of Africa and Asia [1]. Moreover, Sub-Saharan Africa has and will have the world’s highest population growth and urbanisation rates [1] [55].

Existing cities will grow within their current borders and beyond. This “process by which rural areas located on the outskirts of established cities become more urban in character, in physical, economic, and social terms” is called peri-urbanisation [1] [65].

The rapid (peri-)urbanisation has a negative effect on the environment, land use, and land cover. Natural rural vegetation such as forestland decreases and is replaced by urban/built-up areas. Studies show that land use and land cover in the Kumasi Metropolis changed significantly with the ongoing urbanisation [26] [27] [20].

According to Frimpongs study [26] the urban/built-up areas that covered approximately 15% of the Kumasi Metropolis and its adjoining municipalities Asokore Mampong and Atwima Nwabiagya in 1986 increased to 30.68% in 2022. In the rural parts of the metropolis, forest cover has transformed into agricultural land, increasing from 19.47% in 1986 to 42.71% in 2022. Forestlands that covered 65.15% in 1986 were reduced to 26.17% in 2022. The smallest change is seen in waterbodies that slightly increased from 0.33% in 1986 to 0.44% in 2022 (see Figure 2.3a). The loss of biodiversity, soil degradation, and soil erosion are other results of urbanisation.

In another study [27] focusing on the Kumasi Metropolis, the total extent of the built-up area of the metropolis was 128 km^2 in the year 2000. This increased to 171 km^2 in 2010 and 179 km^2 in 2020 (Figure 2.3b). This is an increase of built-up area of 39.8% from 2000 to 2020.

A third study [1] shows that urban land use increased by 54.6% between 1986 and 2016, whilst arable land declined by 15.6% over the same period.

All these changes in land use and land cover make the ground more impermeable for rainwater to naturally infiltrate into the subsurface resulting in a lower natural recharge of the groundwater reservoir in Kumasi [37] [47].

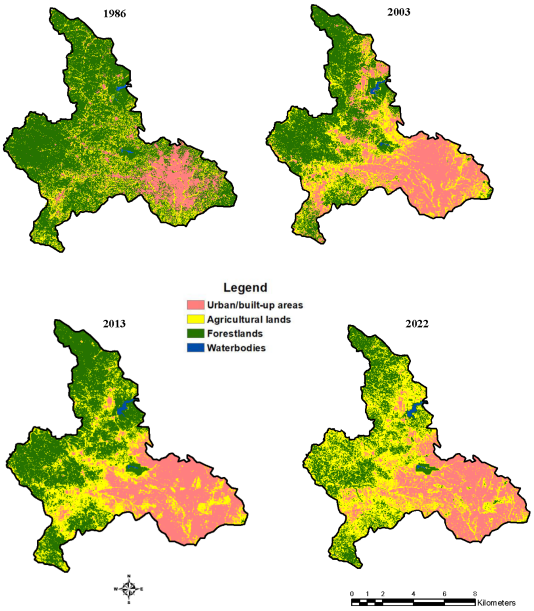

(a) Map of land use changes in the Kumasi Metropolitan Assembly, Asokore Mampong Municipality, and Atwima Nwabiagya Municipality [26].

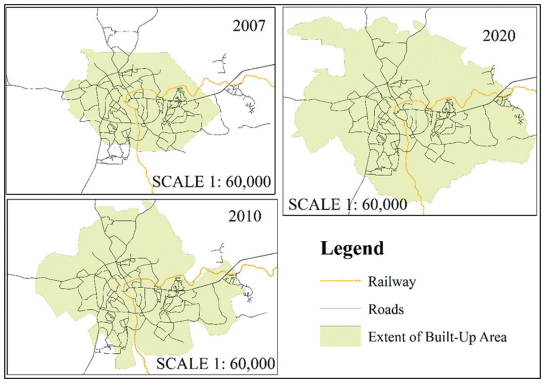

(b) Map of urban extention of the Kumasi Metropolis [27].

Figure 2.3: Maps showing different parts of Kumasi’s urbanisation. Rapid expansion of urban areas is visible.

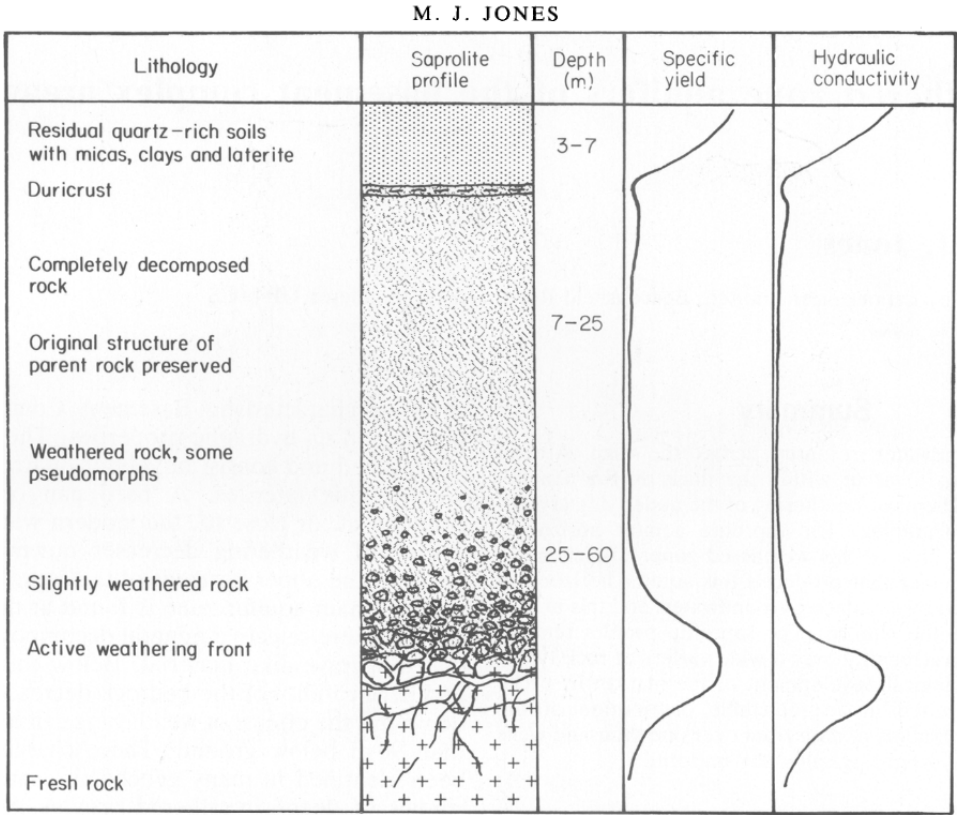

Figure 2.4: The saprolite can be divided into three sections: the top (3-7m), middle (7-25m) and bottom (25-60m). The bottom section has the highest hydraulic conductivity, and thus water content [35].

2.2. Water Availability in Kumasi

2.2.1. Aquifer and Soil Properties

Groundwater is primarily extracted from shallow boreholes and hand-dug wells targeting the aquifer underneath the permeable overburden. This overburden is formed by in-situ chemical weathering of the underlying crystalline basement complex [35]. Chemical weathering is heavily controlled by circulating groundwater through the rock, causing hydrothermal alterations. This groundwater is supplied by precipitation and therefore a function of the climate [3] [35].

The overburden layer, also called the saprolite, tends to have horizontally uniform characteristics, but varies in properties vertically. The saprolite is divided into three sections (Figure 2.4). As is seen in the figure, the lowest hydraulic conductivity is found at the middle section of the saprolite. Here, the rock is completely decomposed, and will have a higher clay content as a result, making flow more difficult through the middle section [44] [35]. Therefore, it is expected that the water table is present around the boundary between the middle and lower section. Local variations of the groundwater flow are a function of slight variations of the hydraulic conductivity and the topography, where groundwater tends to flow from high elevations to lower elevations [69] [70].

The hydraulic conductivity of the saprolite is in the order of 0.01 to 10 meters per day [35]. The saprolite in Kumasi and the surrounding area is expected to be clayey to silty sands [6], where the lithology is mostly determined by the underlying crystalline basement complex [5] [69]. Therefore, it is important to understand the regional geology of Kumasi and the surrounding area (see Figure 2.5 and 2.6).

To the west of Kumasi, Cape-Coast type granitoids can be expected [36]. The granitoids consist of amphibolite marbles, calc-silicates, quartz-mica schists, hornblende schists, greywacke, and feldsparic sandstones and are of the Eburnean Plutonic Suite [44]. To the east of Kumasi, Birimian metasedimentary rocks are found, where the upper Birimian are basalts with interflow sediments [21] [39], and the lower Birimian consists mainly of fine grained rocks with large volcanoclastics, shales, siltstones, and

greywacke [21] [44] [36]. The rocks have been heavily deformed and metamorphised throughout the geologic evolution of the area.

The formation of the geology as it currently is, started with the break-up of the Archean São Luis Craton 2350-2300 million years ago (Ma) (Figure 2.5 Stage 1) [40] [13]. The break-up was followed by rifting, causing extensive magmatic activity (Figure 2.5 Stage 2), later forming the first segments of the West African continental crust such as the Ashanti belt 2350-2150 Ma (Figure 2.5 Stage 3) [31] [40] [25] . As the rifting in the original break-up point continued throughout 2150-2100 Ma, subduction under the West African continental crust made room for the backarc basin known today as the Kumasi Basin. Additionally, the subduction led to the Eburnean Orogeny, which is typically divided into two phases. The first phase relates to crustal thickening as a result of the NW-SE compression between 2130-2100 Ma [33], causing folding, thrust faults and foliation with their strike along the NE/SW (Figure 2.5 and 2.6 Stage 4-5a) [21] . The second phase entailed strike-slip movement, leading to shearing along the pre-existing thrust faults between 2100-1980 Ma [33] (Figure 2.6 Stage 6). Though there is controversy on the timing of the granitoid intrusion specifically, it is theorized that the granitoids intruded the Birimian sediments around the first phase of the Eburnean Orogeny [39] [21] [13]. After this, continuous uplift due to the regional compressional stress field and erosion through chemical and mechanical weathering exposed the rock.

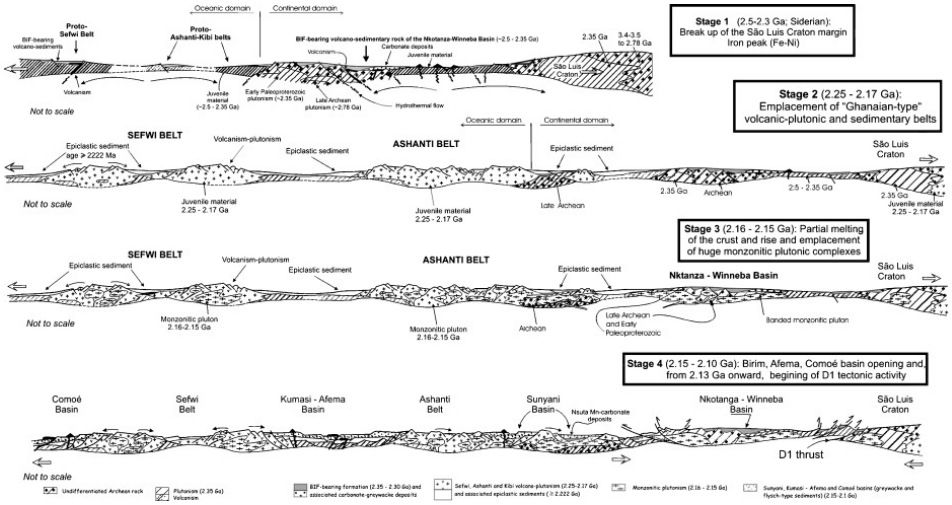

Figure 2.5: Part one of the geological evolution of the Ghanaian province [25].

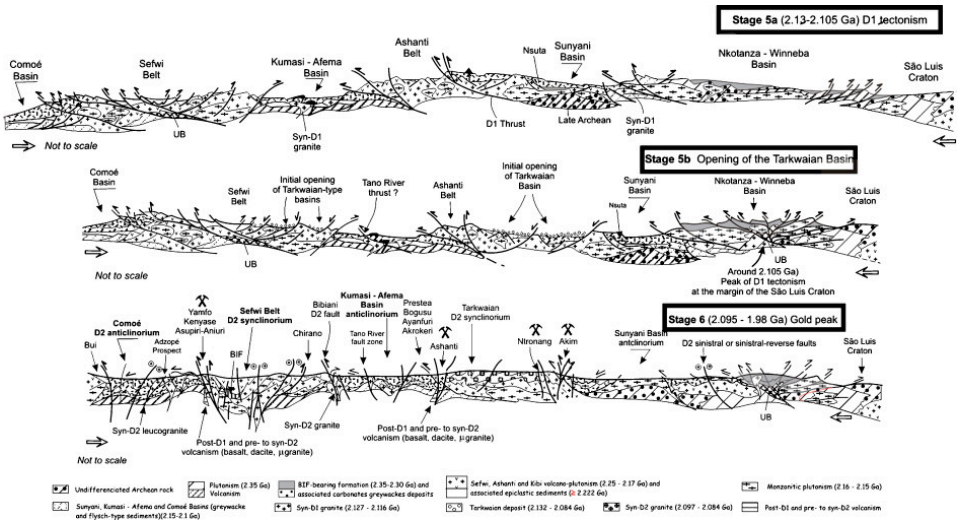

Figure 2.6: Part two of the geological evolution of the Ghanaian province [25].

2.2.2. Water Infrastructure and Groundwater Availability

As the metropolis of Kumasi continues to grow, it is of importance to assess the water availability in this area, to see in what extent the water demand can be met. The Offin and Owabi rivers and their watersheds are a major water supply to the area. Two water treatments plants obtain their water from these rivers, located at Owabi an Barekese [16] (Figure 2.7a).

The piped water system WSS in the Kumasi Metropolis (Figure 2.7b), together with groundwater are the primary water sources for domestic use [29], though access to piped water is as limited as 23% throughout multiple communities as of 2024 [8]. The piped water system does not extend to large parts of the metropolis, especially the newer suburbs and these therefore rely heavily on groundwater.

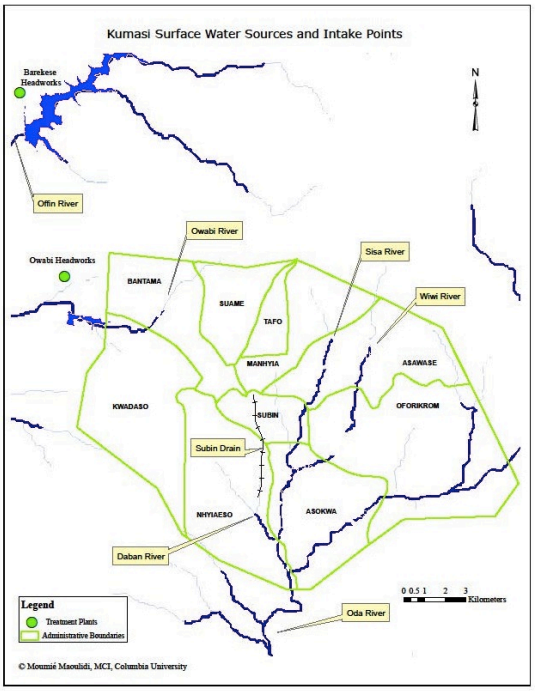

(a) Above shows surface water sources and intake points in Kumasi. Most of the water used in the city is obtained from rivers, such as the Offin and Owabi.

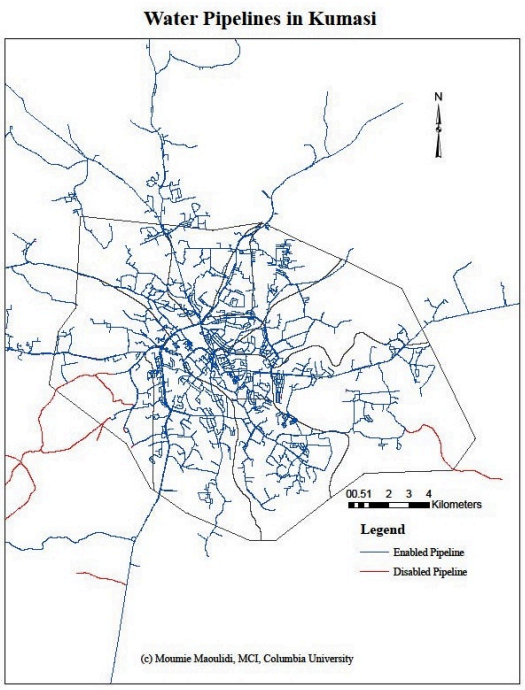

(b) The Kumasi Water Supply System (WSS) consists of more than 1,005 km of pipeline. The map above shows the functioning (blue) and non-functioning (red) water pipelines in Kumasi.

Figure 2.7: Source [16]

According to a survey by Jan Geleijnse in 2022, 61% of residents make use of either boreholes, public boreholes, or dug wells in their domestic households [28]. In the areas used in this report, 100% of the households (partially) make use of groundwater in the Asabi suburb, while only 45% of the households use groundwater in the Edwenase suburb. The households reason that this water supply has the best reliability-quality-price trade-off, though installing a borehole is expensive. In contrast, the WSS is known to be more expensive, notoriously unreliable, and unavailable outside the center. The pipes used are often old and tend to burst, leading to serious (temporary) loss of water supply [45]. Combined, these factors result in a rapid growth in groundwater exploitation as a main source of water. Together with less recharge this leads to significant - largely unmonitored - aquifer depletion.

In addition to the increasing depletion, urbanisation also leads to reduced natural recharge of the aquifer; direct infiltration of precipitation through the weathered overburden is significantly hindered by impermeable pavement compared to green permeable land cover [48]. From 1986 to 2020, the groundwater recharge has decreased by 80%. As a result, as of 2020, the groundwater consumption exceeds the recharge by 2.2 Mm^3 [48]. Extrapolating this trend, by 2050 it is speculated that the groundwater recharge is reduced by 10% due to climate change and by an additional 55% due to land-cover changes [48]. Therefore, new sources of aquifer recharge, management, and regulations should be investigated. While the general public might acknowledge the problem, most people in the Kumasi area state they are not willing to pay to aid in groundwater recharge efforts [28].

2.2.3. Managed Aquifer Recharge

To achieve a sustainable groundwater usage, managed aquifer recharge is a potential technology to scale up in order to increase recharge. “Managed aquifer recharge (MAR) is the purposeful recharge of water to aquifers for subsequent recovery or environmental benefit” [19].

The type of MAR investigated here is rainwater harvesting systems (RWHS) from rooftops. A schematic overview of the difference between wells with and without rainwater harvesting systems and its water-flows can be seen in Figure 2.8.
The left shows a well connected to a RWHS. The rainwater from the roof is collected and directed into the well via roof gutter and pipes. The system is designed in such a way that there is a valve between roof gutter and the pipe into the well. Initially the valve is closed so that the first flush of rainwater, containing all the dust and dirt from the roof, will not reach the well. After this first flush, if the home owner considers the water clean enough, the valve can be opened and rainwater will recharge the well. Next to this direct recharge from the RWHS there is recharge from soil drainage and discharge from soil infiltration and consumption.
The right shows a well that is not connected to a RWHS and is only recharged via natural infiltration and has discharge from soil infiltration and consumption.

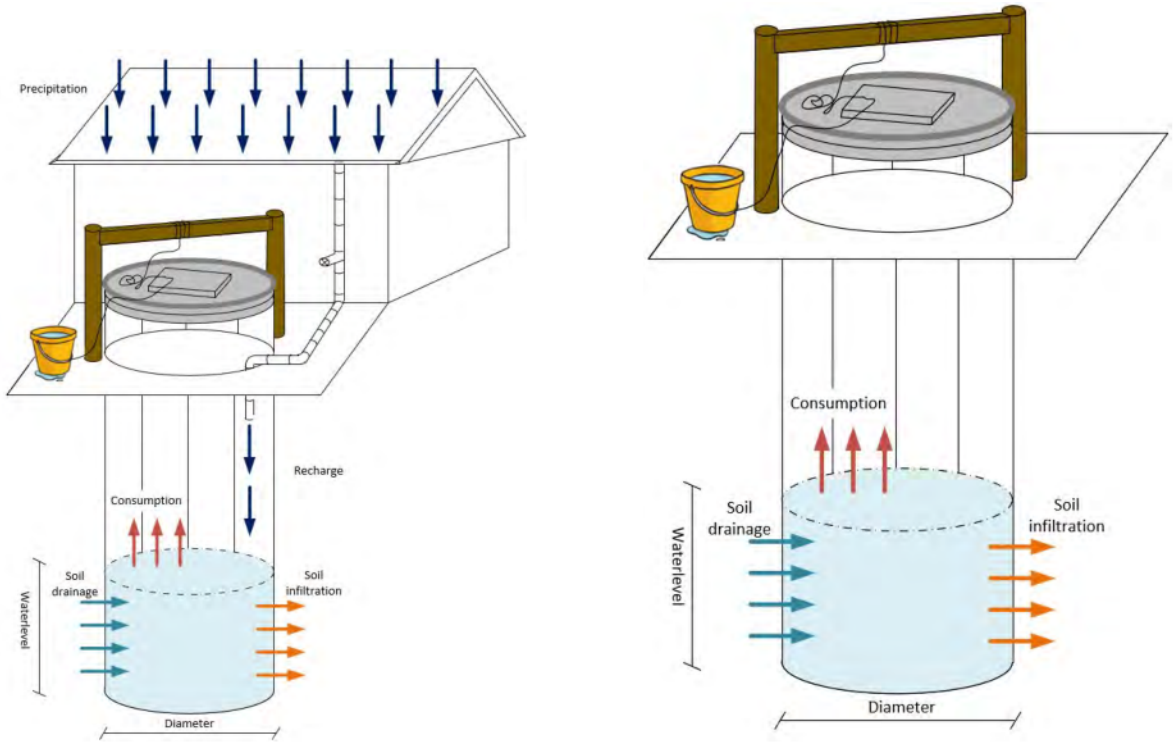

Figure 2.8: Schematic overview of a groundwater well with (left) and without (right) a rooftop rainwater harvesting system [9].

According to Jing et al. “rainwater is usually one of the cleanest available water sources and RWH is one of the best methods available for establishing sustainable water cycles in urban developments” [34].

The performance of RWHS heavily depends on local climate conditions [4] [34] [49]. In areas with a humid climate with high annual rainfall amounts, RWHS are the most effective in storing water, while in dryer climates with lower annual rainfall amounts, RWHS are less effective to store water but are highly effective for stormwater management [4]. Moreover, the performance of RWHS is also impacted by catchment areas, e.g., rooftop area, by tank volume and by water consumption patterns [34] [4].

A study from Jing et al. showed that in general, highest efficiency and reliability are achieved for RWHS in humid climates with larger storage capacities and lower water demand [34]. Almeida et al. showed that the RWH efficiency ranges from 46.56% to 69.97% for a region with the same climate as Kumasi

and a comparable amount of annual rainfall, 1315 mm in Kumasi vs. 1738 mm in Boa Vista, Brazil [4]. However, Almeida found the highest efficiency for a high consumption scenario which contradicts Jing et al.'s findings. Supplying at least 75% of the non-potable water demand was shown to be achieved 45% of the time for smaller roof areas of around 60 m^2 and 70% for larger roof areas of around 240 m^2 [49].

Since these studies are done in a climate similar to Kumasi, the MAR systems in Kumasi are expected to have a comparable effect as the ones in the studies. This shows that MAR has a potential to be of great help in solving the current groundwater depletion.

3

Methodology

In this project, an analysis on the influence of precipitation and Managed Aquifer Recharge was conducted and groundwater levels and groundwater flow were simulated with five MODFLOW 6 models. These models can give insight into changes in groundwater over time and possible groundwater depletion in Kumasi. Groundwater level data from two different areas in Kumasi were analysed together with precipitation data from two weather stations of the Trans-African Hydro-Meteorological Observatory (TAHMO) and fed into the MODFLOW 6 groundwater flow models. In one of the areas, groundwater levels have been monitored for over a year as a pilot project, while the second location only has a data collection for 28 days. The pilot project will be referred to as the pilot site with pilot wells. The site without MAR is referred to as the MDP site, containing the MDP wells.

To gain a better estimate of the effect of MAR, a Compressible Single Phase Connection-based 2D Simulator was developed as well, and was supposed to provide comparison to the MODFLOW 6 models. The simulator works differently from MODFLOW 6 mainly by only taking into account the MAR without natural recharge and treating the MAR systems as injection wells based on pressure instead of groundwater flow. Unfortunately, since this model was built from scratch, the project time was not sufficient for the 2D Simulator to succeed in modelling groundwater flow, but it did give valuable insights which will be discussed in chapter 5.

The whole process from raw data to analysis and model results is shown in a flowchart in Figure 3.1.

3.1. Data Availability

Since the already existing monitoring site is located southwest of Kumasi, a second location was chosen in the north-east region Asokore Mampong as a new monitoring location in the peri-urban area of Kumasi. The two monitoring areas are shown in Figure 3.2, the yellow markers indicating the wells at the pilot project site, the red markers indicating the wells at the new site and the two blue markers are the locations of the TAHMO weather stations. On Figure 3.3 The two measurement areas can be seen in detail.

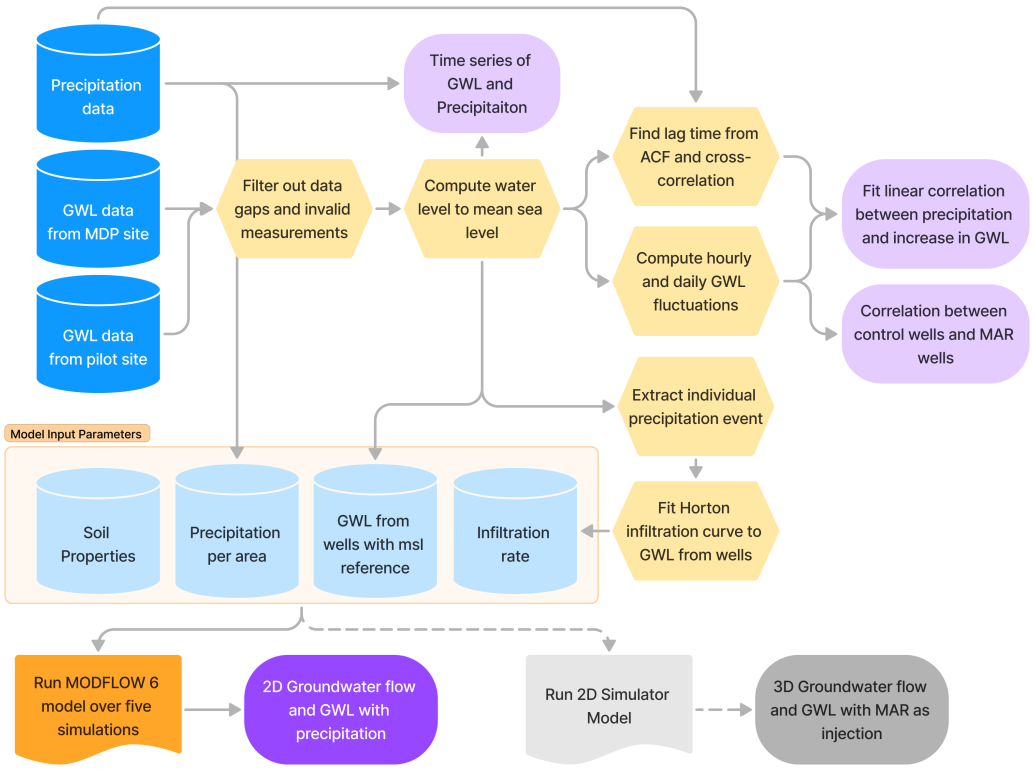

Figure 3.1: Flowchart of the analysis and model process from raw data (deep blue), to data processing in python (yellow), intermediate results (light purple), processed datasets (light blue), model runs (orange) and final results (deep purple). The 2D Simulator model that did not succeed is shown in grey.

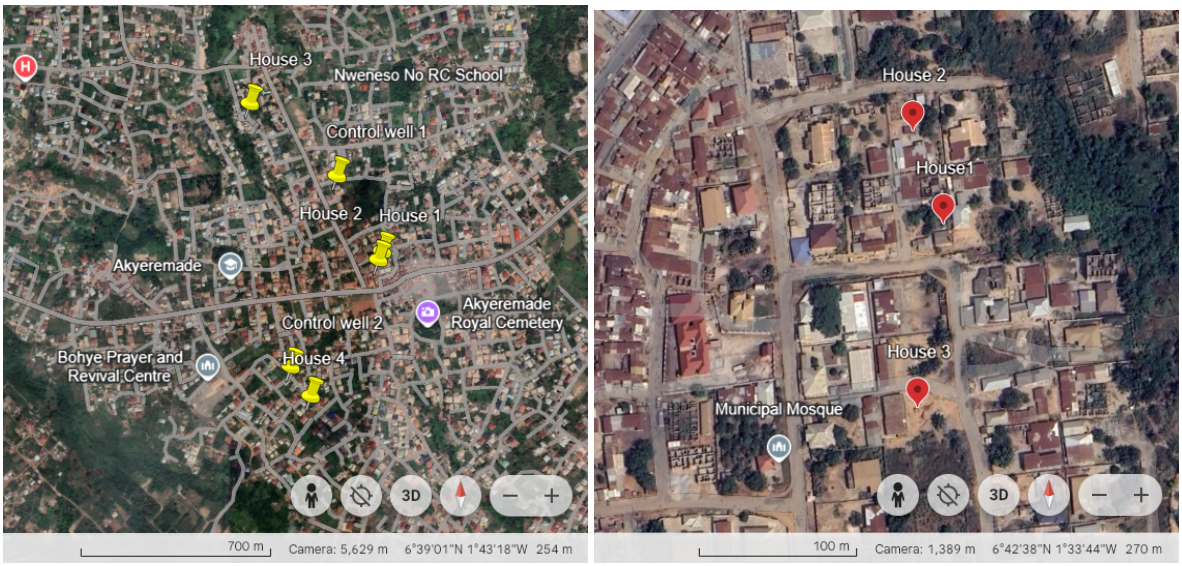

(a) Pilot area.

(b) MDP area.

Figure 3.3: Google Earth map zoomed in on the pilot and MDP area.

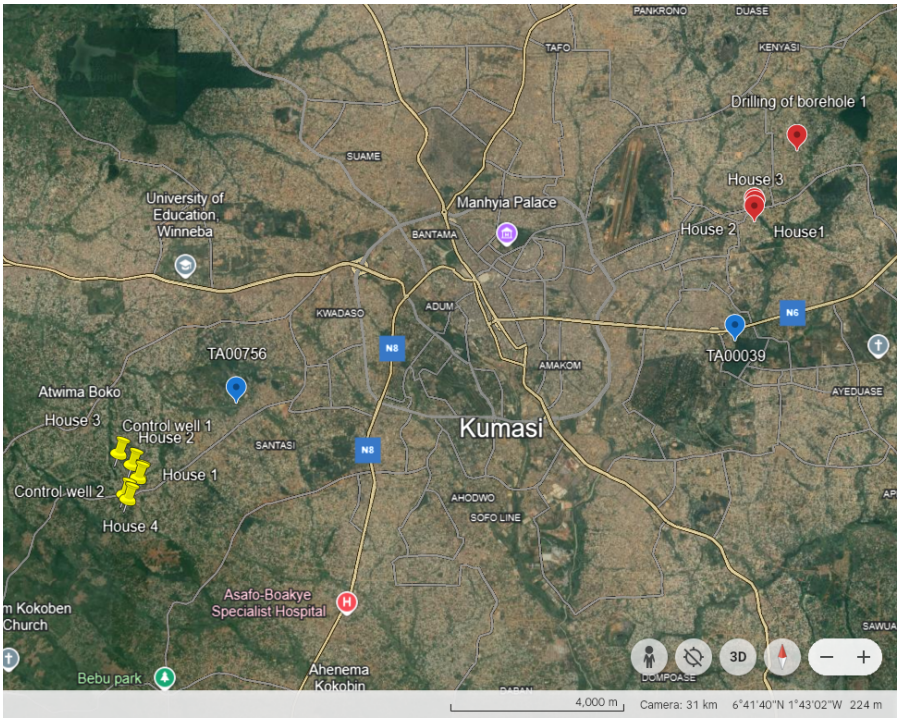

Figure 3.2: Google Earth map of Kumasi with all monitoring locations. In yellow are the pilot project divers and in red the divers installed for this research. The two TAHMO weather stations used in this project are marked in blue [56].

3.1.1. Pilot Project Measurements

As of 2023 a pilot project on Managed Aquifer Recharge from the Kwame Nkrumah University of Science and Technology (KNUST) has been ongoing, where originally eight hand dug wells were monitored of which now six are still operating as part of the project [9]. They are located south-west of Kumasi in a peri-urban area (yellow markers in Figure 3.2) and provide water to several households each. Four of the six remaining wells are equipped with a rooftop RWHS, while the other two wells serve as control wells without artificial groundwater recharge. These six wells serve as our measuring site with MAR influence (Table 3.1).

Each well is equipped with a vanEssen CTD-Diver to monitor the water level in the wells on an hourly basis from June 2023 to September 2024, and at five minute intervals from September 19th 2024 to October 17th 2024. The time resolution of the measurement was changed to analyse the response of groundwater levels to precipitation events on short time scales. As can be seen in Figure 3.4, the divers are installed at the bottom of the wells at a depth such that they should be continuously submerged in water even at low groundwater levels. They measure the absolute pressure exerted by the atmosphere and the water column above the diver.

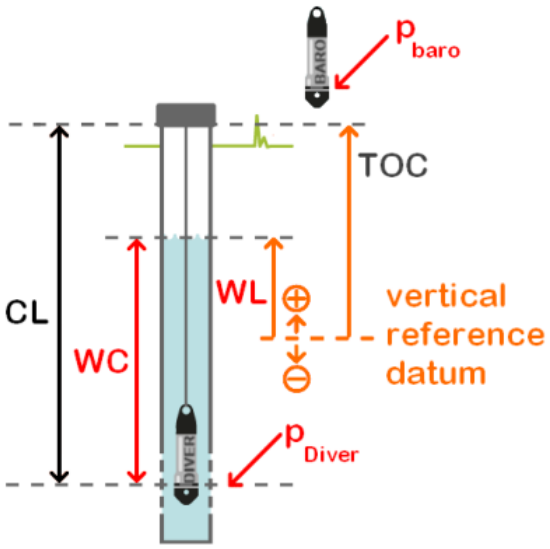

Figure 3.4: Diver installation from product manual [62].

In order to obtain the water column height (WC [m]), one of the control wells is equipped with a barometer to measure the atmospheric pressure for compensation ($p_{\texttt{baro}}$ [hPa]). The diver data is compensated to remove the atmospheric pressure from the total pressure measured by the diver ($p_{\texttt{Diver}}$ [hPa]), from which the water column is found as follows:

$$WC = 9806.65 \frac{p_{\texttt{Diver}} - p_{\texttt{baro}}}{\rho g} \tag{3.1}$$

Here ρ [kg/m^3] and g [m/s^2] are the density of water and the gravitational acceleration respectively. The groundwater level (WL [m]) with reference to mean sea level can then be calculated:

$$WL = WC + TOC - CL + G_{\texttt{el}} \tag{3.2}$$

where TOC is the top of the well casing in meters, CL is the cable length at which the diver is suspended at in meters, and $G_{\texttt{el}}$ is the ground elevation above mean sea level in meters, which is used as our vertical reference datum.

The wells were visited regularly for maintenance and to obtain the new data gathered. Since this is the longest data record of groundwater levels in Kumasi available for this report, it serves as a foundation for the analysis of groundwater levels under the influence of MAR.

3.1.2. Additional Groundwater Monitoring System

The second area was monitored from September 19th to October 17th 2024. Here, three monitoring wells without MAR systems were chosen within 1 km^2 area from each other, after which one vanEssen diver was installed in each, as well as one barometer as atmospheric pressure reference. The barometer was installed in a well that is not used by the owners anymore, which gives a reliable measurement record without human interruptions. The locations of the monitoring wells can be seen on the map in Figure 3.2 and the specifications of each well are shown in Table 3.1. The elevation is slightly different here, and the new site is partly water logged, while the pilot project site is not.

Table 3.1: Specifications of the nine monitoring wells.

	MDP well 1 (MW1)	MDP well 2 (MW2)	MDP well 3 (MW3)	Control well 1 (CW1)	Control well 2 (CW2)	Pilot well 1 (PW1)	Pilot well 2 (PW2)	Pilot well 3 (PW3)	Pilot well 4 (PW4)
Well depth [m]	4.51	8.05	8.32	-	19.2	20.7	20	3.7	9.2
Water level from bottom [m]	0.98	2.96	0.34	0.8	1.5	1.1	1	2	1.5
Top of Casing (above ground) [m]	0.59	0.60	1.49	0.4	0.3	0.6	0.2	0.5	0.2
Cable length [m]	3.90	6.92	8.14	12.02	18	19.78	19.05	2.97	8.9
Ground elevation above mean sea level [m]	270.61	271.50	275.58	263.90	269.60	274.04	273.63	244.26	265.09
Well diameter [cm]	82	90	94	100	100	90	100	100	95
Well area [m^2]	0.528	0.636	0.694	0.785	0.785	0.636	0.785	0.785	0.709

3.1.3. TAHMO Weather Stations

TAHMO provides weather data through a network of currently 9.000 weather stations across Sub-Saharan Africa. Their goal is to improve the monitoring and availability of weather data across Africa for monitoring as well as agricultural purposes [56]. Each weather station can measure the air temperature, precipitation and pressure as well as other quantities not relevant for this project. The precipitation is measured in mm with a temporal resolution of five minutes and was also obtained as hourly data to match the groundwater level data.

In this project, two TAHMO weather stations located nearest to each of the two measuring sites were chosen (blue markers in Figure 3.2), to represent the precipitation at the well locations as true as possible. One weather station is located at the Kwadaso Agricultural College, 3.1 km from the pilot project site and the other station is located at the KNUST Junior High School, 2.8 km from the MDP project site. The rainfall data was obtained online and used for the analysis of the corresponding site.

3.2. Groundwater Level and its Relation to Precipitation

Groundwater in Kumasi is largely recharged by infiltration from rainwater. This infiltration is natural, while MAR enhances the effect precipitation has on the water levels. This effect can give an indication of the effectiveness of MAR and of the effect of natural infiltration.

3.2.1. Filtering the Groundwater Level Data

The correlation between the groundwater level and precipitation is calculated in order to assess the relation between the two. However, the data contains noise and measurement errors, partly due to instances where the divers were not constantly submerged in the water because of lowered water levels. For this reason, a filtering process is implemented. The filtering consists of several steps:

- Conductivity less than 0.005 milliSiemens per centimeter [mS/cm]: a conductivity close to zero indicates that the diver measured the conductivity of air and not the conductivity of water, which is expected in the range of 0.2-0.8 mS/cm for drinking water [38];
- Water column less than 0.05 meters: the diver was assumed to be out of the water at this point. The threshold was set at 5 cm, even though the diver accuracy is ± 1 cm, since the water column above the diver is calculated based on the pressure measured by the diver and the barometer, where the latter can vary as a result of noise and therefore cause artifacts in the measured water column;
- The vanEssen divers can measure water columns up to 10 m, thus measurements exceeding this range were filtered out accordingly;
- Due to water being extracted up to several times a day, a lot of drops in water level were present in the data. These act as noise in the data, especially for comparison with the precipitation data.

Through filtering out short-lived drops in water level the amount of noise from extraction events is reduced, but many smaller extraction events are not possible to distinguish and remove in this way.

To obtain a common reference for all wells, necessary for the later comparison and modeling, the groundwater levels were calculated with reference to mean sea level, using Equation 3.2. Here, the top of the casing of the wells and the cable lengths were measured on site. The ground elevation of each well was determined using the Copernicus Digital Elevation Model (DEM), a digital surface model provided by the European Space Agency through Digital Earth Africa [18], which offers a horizontal resolution of 30 meters. This spatial resolution is lower than the modelling grid, but this is sufficient given the low amount of data points in the models and large scale of the groundwater modelling area.

3.2.2. Correlation between Precipitation and Delayed Response of Groundwater Level

The filtered water level was plotted as a time series along with the precipitation. For the long-term data set, the daily sum of precipitation from TAHMO was computed and compared to daily mean water level for all of the wells. Furthermore, the correlation between water level variations and the precipitation from TAHMO was determined.

As not only the most recent rainfall event has an effect on the groundwater [66], but also the previous rainfall events [54], it is necessary to account for the lag when calculating the correlation between the rainfall and the groundwater level. First, the auto correlation function of the groundwater itself and the resulting lags were investigated. Secondly, the water level differences and precipitation were cross-correlated for different lags, identifying the optimal lag time where the correlation is strongest. The correlation between control wells and MAR wells was also plotted to validate that the groundwater level in both the control wells and the MAR wells behave similarly in time.

Using the hourly data obtained at the pilot site over 16 months, a method proposed by Chyan-Deng Jan et al. (2007) [32] on the effect of rainfall on groundwater level increment was applied in a slightly modified version. For this method, the daily differences in groundwater level were calculated from the water level at the beginning and the end of each day for a one-month period with many rainfall events. After finding the period when no rainfall event occurs, the average decrease rate in water level, called recession rate, was subtracted from the daily water level difference. From here, the correlation between the daily water level difference and daily sum of precipitation was calculated for each pilot well. The obtained correlation coefficients and the fitted regression lines serve as validation for the models, which assume a positive relation between precipitation and water level increases.

3.3. Groundwater Flow and Level Models

The workflow of geohydrological modelling uses the simulation software MODFLOW 6 and the python package Flopy in order to obtain the groundwater level and flow in 3D over time. MODFLOW 6 uses process-based simulation resulting in cell-by-cell flow. It is user friendly and computationally inexpensive compared to other groundwater flow models. Different input parameters, such as (local or regional) recharge through precipitation, can be added. The setup of the MODFLOW 6 models is as follows:

- An irregular, structured grid is used below the surface elevation.
- Two layers are defined based on the primary soil data and literature. These values are different in the MDP site and pilot site. The layers are uniform in thickness over the whole area and have an isotropic hydraulic conductivity, meaning that the water can flow equally in all directions.
- The model is treated as an open system with no boundary conditions at the side and bottom interfaces, such that the outflow varies with the modelled groundwater flow.

The extrapolation outside of the known points (the wells) is minimized by taking the boundaries of the model relatively close to the wells itself. Some space is still left to ensure that the boundary conditions would not influence the model results in large extents.

3.3.1. Co-kriging

To simulate the initial groundwater level across both regions, co-kriging is used between the elevation and the initial hydraulic head levels in the wells. Multiple studies suggest that the topography of an area can greatly influence the groundwater level and should therefore be incorporated via, for instance, collocated kriging [14] [42] [71]. In this method, the groundwater level serves as the primary variable to be interpolated, while elevation acts as the secondary variable that helps guide and improve the simulation of the primary variable.

As only six points have been measured throughout a research area of roughly 0.7 km^2 at the pilot site and three points throughout 0.06 km^2 at the MDP site, an interpolation method was needed in order to obtain a static groundwater level over the whole area. A Pearson correlation analysis of 0.67 shows a relationship between the two variables [10]. This coefficient is sufficiently high to support the implementation of co-kriging with the topography of each area and use the result as initial condition for the five MODFLOW 6 models.

3.3.2. Groundwater Level and Flow Modelling using MODFLOW 6

MODFLOW 6 is a program from the U.S. Geological Survey and can be used to simulate and predict groundwater conditions [58]. Stress periods can be added to simulate periods of transient hydraulic head, recharge, outflow, and more. Five MODFLOW 6 models have been made using the Flopy (MODFLOW 6) package in python, all with slightly different focus areas:

- The pilot site, using precipitation and hydraulic head data over the past 16 months (from June 2023 - September 2024). The hourly data collected for this has been filtered and averaged per month, hoping to see seasonal changes in groundwater flow.
- The pilot site utilizes data collected at five minute intervals between 19-09-2024 and 17-10-2024 to observe the potential effects of MAR. It is anticipated that the impact of MAR will be evident over this period.
- The MDP diver site, using the data in five minute intervals obtained from 19-09-2024 to 17-10-2024. The difference between MAR and no MAR can be seen when comparing this to the former model.
- The pilot site around a single rainfall event. This is to see the infiltration rates and the short term effects of MAR and natural recharge on the groundwater level.
- The MDP diver site around a single rain event to see the infiltration rates without MAR. Also, the difference in response between this water logged area and the pilot site is analyzed.

Figure 3.5 summarizes all types of input parameters, while Table 3.2 shows the general input values. The grid for the pilot site is 600m x 1200m, which translates to a 50 x 100 cell grid. The MDP diver site has sizes of 200m x 300m, where a finer grid of 100 x 150 cells has been defined. All grids have two defined layers: the less permeable decomposed part of the saprolite (25m), and the coarser, more permeable part of the saprolite, closer to the crystalline basement (8m). The thicknesses are based on differences in calculated hydraulic conductivity of soil samples, and the overburden thickness estimates of Ewusi et al. [23]. The Copernicus DEM defines the ground surface of the sites, under which the two layers have a constant thickness. Each layer is set to have an isotropic, homogeneous hydraulic conductivity and is set to be incompressible [7]. As an unconfined aquifer is modelled, the specific yield and specific storage need to be determined. As no primary data is available, values from literature are used [41] [2] [11]. The initial condition for the hydraulic head is given by the model obtained by co-kriging, as explained in 3.3.1.

In the first model, the daily accumulated rainfall is added using the recharge package over the top of the grid [48]. The monitored wells are inserted in the grids, the initial hydraulic head is added, and the time-varying head is defined using daily data. Each day is defined as a ‘transient’ stress period.

In the second and third model, the stress periods are five minutes long, as this is the same as the temporal resolution of the data gathering. The total simulation time is 28 days. The rain is also added as five minute intervals of steady-state rainfall.

The last two models are simulated over 24 hours with one major occurring rain event. Here stress periods of five minute intervals are applied as well for both the hydraulic heads and precipitation. This

can tell us more about the fine scale dynamics of each site and how the groundwater levels react to precipitation.

Table 3.2: Values for input in MODFLOW 6

	General	
Recharge through precipitation per cell [m/day]	cumulative per month, average: 9.23E-8	
	Pilot site	**MDP site**
Site area [m]	600 x1200	200 x300
Grid size [-]	50 x 100	100 x 150
Well locations [grid cell, from bottom left]	48 x 49 49 x 52 7 x 94 30 x 4 34 x 74 23 x 15	54 x 136 46 x 165 45 x 101
Specific yield [-]	0.02	0.02
Specific storage [cm^{-1}]	5E-6	2E-5
K top layer [m/day]	0.01	1
K bottom layer [m/day]	62.5	62.5
	Top layer	**Bottom layer**
Depth, bottom of layer [m]	model top - 25	model top - 33

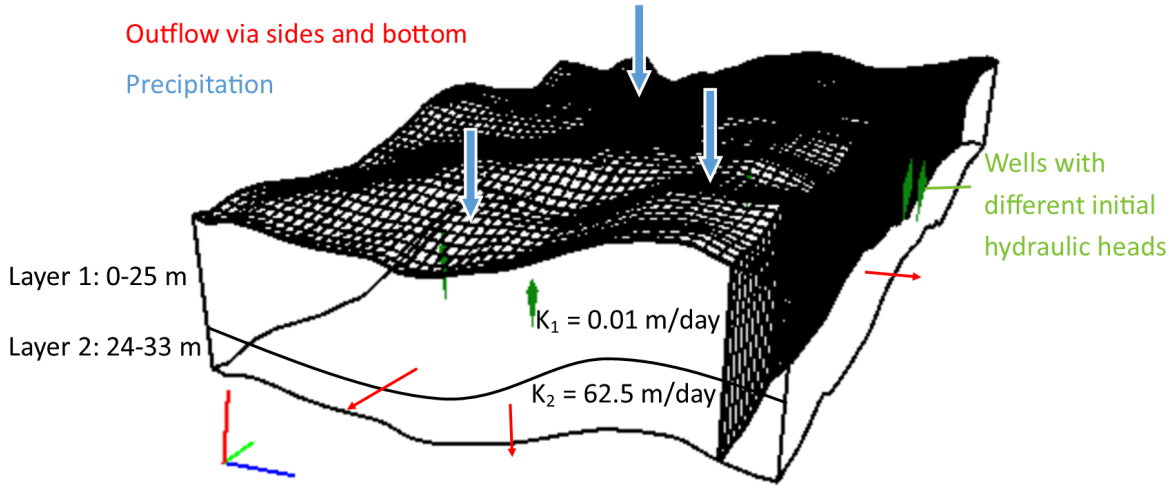

Figure 3.5: Schematized overview of the input parameters for the pilot site in MODFLOW 6.

3.3.3. Hydraulic Conductivity Determination

The hydraulic conductivity is a vital part of the groundwater flow models, as a low hydraulic conductivity will result in slower flow rates and therefore the soil will respond differently to MAR.

Soil samples from a borehole drilling near the MDP monitoring site were collected each meter of drilling (Figure 3.6). As the soil is disturbed during drilling, hydraulic conductivity measurements could not be taken, and are therefore derived from semi-empirical relations with particle size distributions. An analysis of the particle size distribution of most of the samples was done in the geo-technical lab at KNUST. The samples analyzed were at 3, 4, 5, 6, 9, 10, 11, 12, 15, 18, 21, 24, 27, 29 and 31-33 meters, based on an initial visual comparison of soil types (Figure 3.6). In the lab, the samples were first dried

in a 110 °C oven, after which a hydrometer test was done (Figure 3.7). This determines the particle size distribution of silt and clay present in the soil. After washing and drying the samples again, the samples are sieved, determining the coarser particle size distribution. After this, the semi-empirical relation defended by W. D. Carrier is used [12]:

$$k = 1.99\mathrm{E}4 \left(\frac{100\%}{\sum f_i / D_{\mathtt{li}}^{0.404} D_{\mathtt{si}}^{0.595}} \right)^2 \frac{1}{SF^2} \frac{e^3}{(1+e)} \tag{3.3}$$

- k = hydraulic conductivity [m/day]
- f_i = percentage of sample caught in the sieve [%]
- D_i = larger (`l`) and smaller (`s`) diameter of sieve size [m]
- SF = shape factor [-]
- e = void ratio [-]

Assumptions have been made for the void ratio and shape factor based on inspection of the sample. The shape is sub-angular, and based on W.D. Carrier, 7.5 is a typical value for this shape [12]. Furthermore, the sample size classification for all samples points to a sandy-loam. A typical value for the void ratio of a sandy loam is 0.8 [43] [51] [46], so this is assumed for all samples.

As the soil samples were gathered close to the MDP site, the results of the analysis will be adequate for this site. However, the pilot site is located in a different geology. Drilling logs in the area of the pilot site have shown that the upper layer is silty and clayey, which is different from the MDP site. Therefore, a hydraulic conductivity derived from literature has been used [11].

Figure 3.6: Soil samples at the drilling site. The samples are sorted according to depth with the top right sample being the first drilling meter to the bottom left sample at 33 m going column by column. The iron oxidation and visible changes in particle size distribution guided the decision of which samples to analyze.

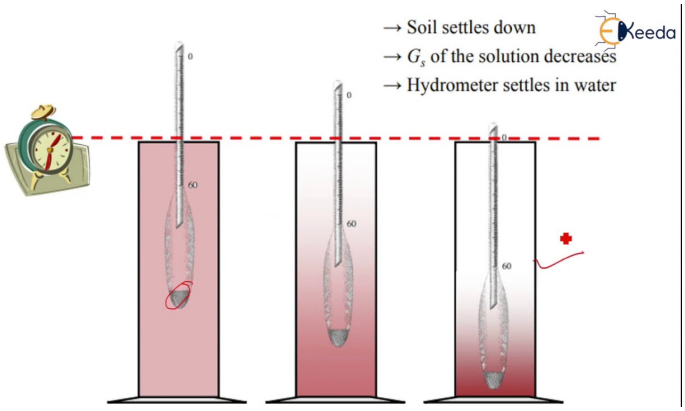

Figure 3.7: Theoretical representation of a hydrometer test. The fine silt and clay particles precipitate at different times after shaking the sample, which influences the density of the water [22].

3.4. Extrapolation of MAR Recharge to the Kumasi Peri-Urban Area

To give an indication of how much depletion is expected in all of the Kumasi peri-urban area, as well as estimating how many wells would be needed with regards to this population size to recharge the groundwater completely, the MAR recharge obtained from the pilot site is extrapolated to the whole peri-urban area. For this, a similar type of MAR system as in the pilot site is assumed to be implemented everywhere. Based on the literary research described in subsection 2.2.1, a horizontally homogeneous overburden in the whole peri-urban area of Kumasi is assumed for the purpose of estimating volumetric groundwater recharge. This assumption is necessary since the other aquifers in Kumasi are largely unknown.

The MAR efficiency is calculated based on the difference in volumetric groundwater change between the pilot site and the MDP site. This volumetric difference will show the net change in water level over the 28 days of measurement, with and without MAR, and is calculated as follows:

$$\Delta V = \frac{1\text{E}6}{A_{\texttt{site}}} A_{\texttt{cell}} \sum_{i=0}^{N} \Delta h_i \tag{3.4}$$

- ΔV = volumetric change over 1 km^2 [m^3/yr]
- $A_{\texttt{cell}}$ = area per cell in model [m^2]
- $A_{\texttt{site}}$ = area of the model extent [m^2]
- Δh = change in hydraulic head [m]
- N = number of timesteps

To be able to compare the volumetric differences in groundwater of the pilot and MDP site, upscaling is needed to get the same area for both regions. Therefore, the equivalent rooftop area for RWHS and number of wells is calculated per km^2. This MAR efficiency is expected to be less than the theoretical one, since the volumetric change is influenced by other factors in the model, however the individual MAR recharge at the pilot wells is unknown, therefore the estimated amount of wells from this method should be viewed as an upper bound.

September and October – when the measurements were taken – are typically in the wet season, while depletion is more likely to occur in the dry season. Therefore, the volumetric change over the entire year is based on a yearly estimate of 31.1 Mm^3 of groundwater consumption and 28.9 Mm^3 of natural recharge from Potter for the entire Kumasi peri-urban area [48]. From the efficiencies and the volumetric changes, a series of calculations leads to the number of wells needed to recharge all of the Kumasi peri-urban area:

$$\eta = \frac{pr \cdot A_{\texttt{roof,km}}}{\Delta V_{\texttt{pilot,28days}} - \Delta V_{\texttt{mdp,28days}}} \tag{3.5}$$

$$A_{\texttt{roof,needed}} = \frac{\Delta V_{\texttt{pilot,year}}}{(\eta \cdot pr)} \tag{3.6}$$

$$N_{\texttt{wells}} = \frac{A_{\texttt{Kumasi}} \cdot N_{\texttt{wells,km}}}{1\text{E}6} \tag{3.7}$$

- η = efficiency of MAR [-]
- pr = precipitation [m/yr]
- $A_{\texttt{roof,km}}$ = rooftop area used in the pilot site, compensated to 1km^2 of ground area [m^2]
- $A_{\texttt{roof,needed}}$ = rooftop area needed to recharge the aquifer in Kumasi [m^2]
- $N_{\texttt{wells}}$ = number of wells needed to recharge the aquifer in Kumasi [-]
- $A_{\texttt{Kumasi}}$ = area of peri-urban Kumasi area [km^2]
- $N_{\texttt{wells,km}}$ = number of wells used in the pilot site, compensated to 1km^2 [km^{-2}]

4

Results

4.1. Water Level and Precipitation

4.1.1. Time Series of Groundwater Level

The time series of hourly groundwater levels at the pilot site over 16 months together with precipitation from the nearby TAHMO weather station in Figure 4.1 show a visible relationship between precipitation events and changes in water level. Spikes in water level at pilot well 1, 3 and 4 clearly coincide with rainfall events, suggesting a direct influence of precipitation on groundwater. During periods of no rain events, the level of groundwater declines due to natural discharge, which is seen in control well 2 in pilot site. Short-lived drops of groundwater level can be attributed to water extraction from the wells.

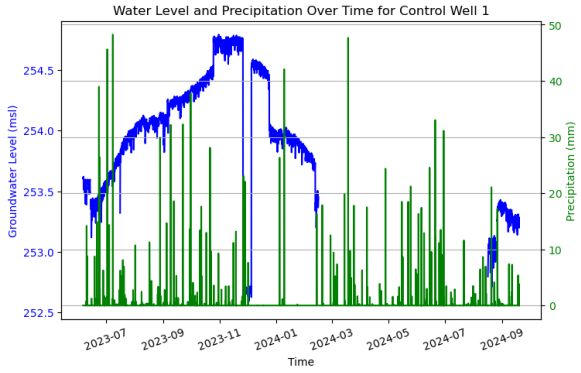

(a) Control well 1

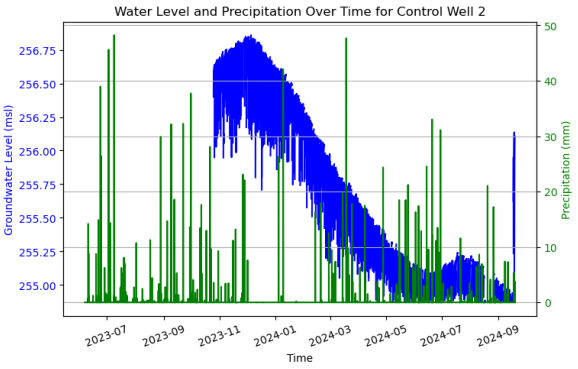

(b) Control well 2

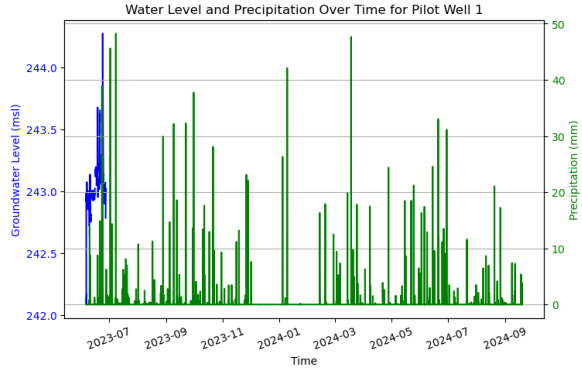

(c) Pilot well 1

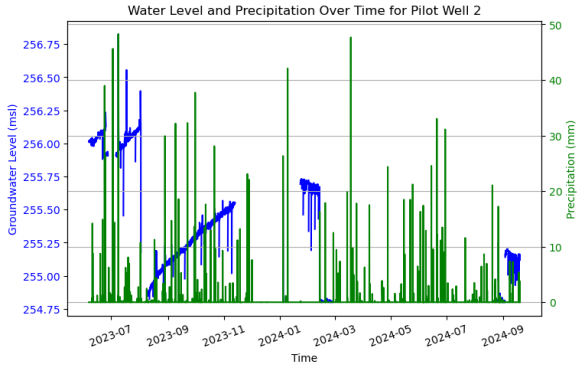

(d) Pilot well 2

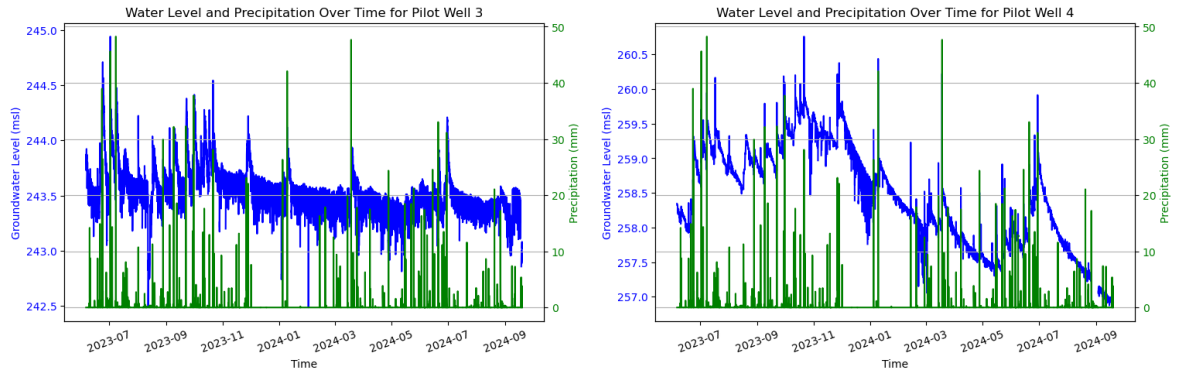

(e) Pilot well 3

(f) Pilot well 4

Figure 4.1: Time series of hourly groundwater level with respect to mean sea level of each pilot well (blue) and the hourly precipitation from TAHMO (green). Note that the water level axes are different.

The groundwater level seems to be quite stable at pilot well 3, while there is a continuous decrease at pilot well 4. This indicates that the water level never reaches steady state. Unfortunately, the time series of pilot well 1 is much shorter due to the diver failing after only one month.

The diver measurements collected every five minutes (Figure 4.2) show an overall increase in groundwater level at pilot well 4 and MDP wells 1, 2 and 3 during the whole measuring period with frequent rainfall. However, the other wells at the pilot site are very disturbed by groundwater extraction events and show no clear increase in groundwater level with precipitation.

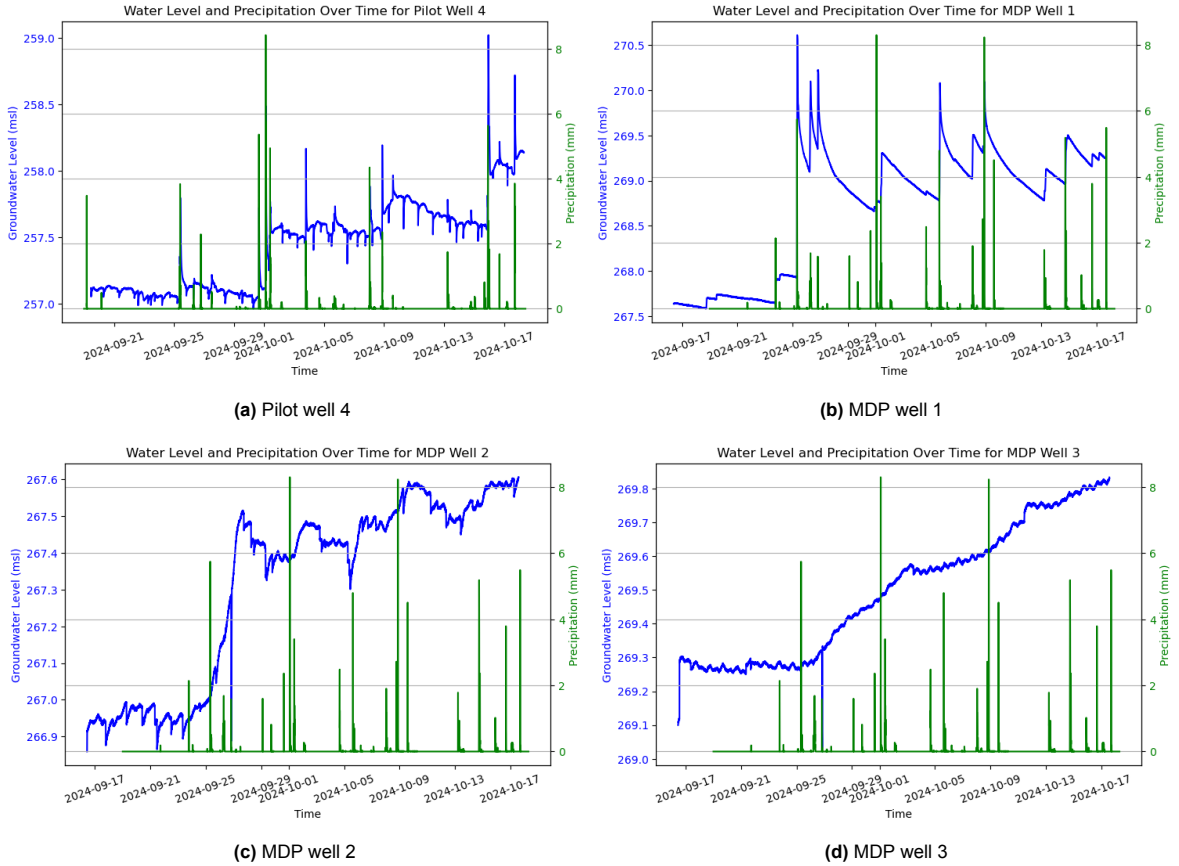

(a) Pilot well 4

(b) MDP well 1

(c) MDP well 2

(d) MDP well 3

Figure 4.2: Time series of groundwater level recorded every five minutes with respect to mean sea level of each pilot and MDP well (blue) and the precipitation collected every five minutes from TAHMO (green), from 19th of September to 17th of October 2024.

At the MDP wells, groundwater levels fluctuate in response to rainfall events, with some showing more immediate changes while others remain more stable over time. The water level in MDP well 1 shows a fast rise, followed by steep drops after rain events. The water level in MDP well 2 responds to rain with slower increases in water level. However, no steep infiltration is noticeable after rain events. In MDP well 3 there is a constant increase in groundwater level after several rain events, which could be explained by a delayed response due to infiltration and groundwater flow from outside of the MDP site towards this area. MDP well 1 tends to react quickly to precipitation events, even though it is not connected to a MAR system. This can likely be explained by the more permeable soil and the water level being much closer beneath the surface than at the pilot site. It is also noticeable that the water level is quite stable before the rain starts, likely an effect of the area being waterlogged, so the groundwater does not flow away.

4.1.2. Correlations

The correlation analysis based on the hourly groundwater level and precipitation data did not show a significant correlation for most of the pilot wells. As the response to precipitation is quick, hourly data lacks the temporal resolution to capture any true correlation. Nevertheless, this is likely also due to infiltration of precipitation into the groundwater, which creates a delay between the time of precipitation and the increase in groundwater level. After accounting for the time lag, we found the optimal lag for each well which give the highest correlation coefficients, however they all show very low correlations. Therefore, a simple correlation analysis proved to be insufficient because of the disturbance due to water extraction and the influence of past values of water level, occurring over longer timescales. This can be confirmed by looking at the autocorrelation function of each well (Figure 4.3).

Table 4.1: Calculated temporal lag in five minute intervals which result in highest Pearson Correlation Coefficient between the precipitation and water level difference between each timestep.

Name of well	Optimal Lag [min]	Pearson Corr. Coeff.	Coeff. Chyan-Deng Jan
Control well 1	5	0.01	0.038
Control well 2	35	0.01	0.198
Pilot well 1	N/A	N/A	N/A
Pilot well 2	10	0.06	0.02
Pilot well 3	40	0.02	0.736
Pilot well 4	5	0.19	0.755
MDP well 1	5	0.25	0.787
MDP well 2	50	0.08	0.617
MDP well 3	25	0.11	0.326

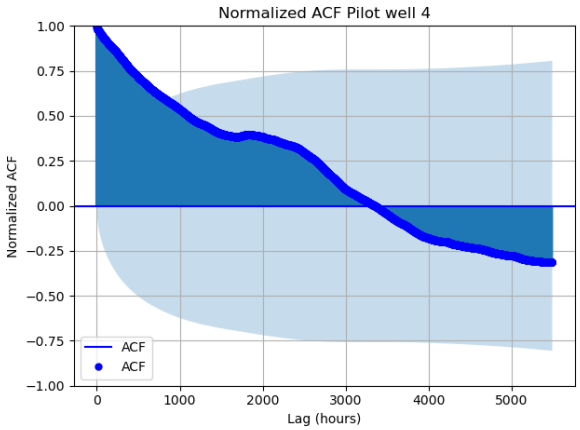

Figure 4.3: Auto-correlation function of pilot well 4 with 95% confidence interval cone in light blue. The hourly lag is outside the confidence interval until a lag of 800 hours, showing a significant time dependence over more than one month. The ACF of other wells look very similar.

To address this, a method proposed by Chyan-Deng Jan et al is employed [32]. This method is less effective at capturing individual rain events than using the hourly data, since the infiltration rate is highest in the first few hours. However, the obtained correlations are higher, as the influence from both the time lag and the noise of water extraction is limited. The Pearson correlation coefficients from this method (Table 4.1) show a positive correlation between daily water level increases and daily precipitation for pilot well 3, pilot well 4, MDP well 1 and MDP well 2. Meanwhile, the correlation between daily precipitation and water level difference for the other wells remains insignificant, for which there are several possible causes. Delayed influence over longer time scales is very likely, since some of these wells are deeper and precipitation takes longer to infiltrate, especially control well 1 and 2. Additionally, it is known that pilot well 2 is less consistent in opening the valve of the RWHS into the well, compared to the other pilot wells, resulting in missing out on the potential recharge.

The change in water level between control well 2 and pilot well 4 of the pilot site is plotted against each other in Figure 4.4 based on the one year measuring period. These two wells were chosen because of their close spatial proximity, similar elevation pattern and continuous data record. Despite a lot of noise, it is clear that the water level of pilot well 4 increases when the water level of control well 2 increases with a linear relationship. From the magnitude of water level rise it can be interpreted that the water level increases slightly more in the well with MAR than in the control well where there is only natural infiltration.

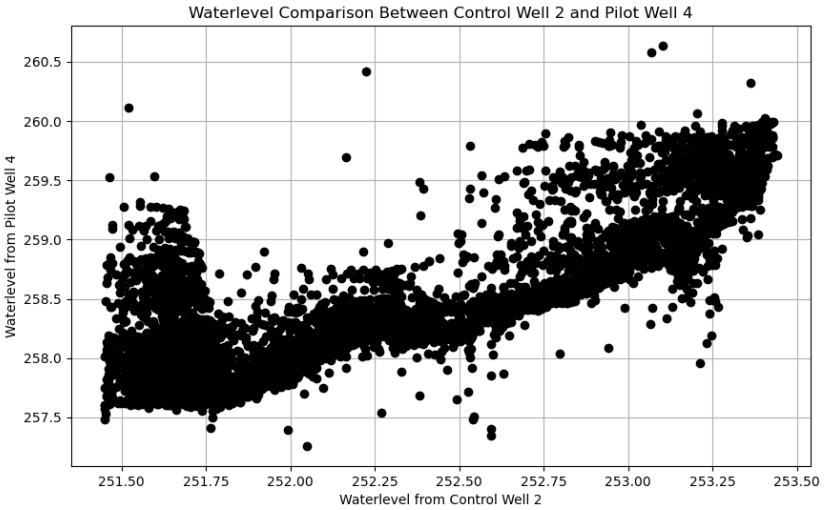

Figure 4.4: Correlation between hourly water level of control well 2 (without MAR) and pilot well 4 (with MAR).

4.1.3. Hydraulic Conductivity

The particle size distribution (Figure 4.5a) seems to be generally constant over the first 24 meters of the saprolite, with a sand content of 14-25% and a silt content of 72-86%, classifying this section as a sandy-loam. The calculated hydraulic conductivity has an average of 1.33 m/day, with a standard deviation of 0.586. However, from 27 to 33 meters, the hydraulic conductivity is much higher, with two out of the three samples in this region being higher than 40 m/day (Figure 4.5b). Too few samples were taken in this area to analyze statistically, though the sharp increase in hydraulic conductivity is noted and incorporated in the groundwater models. This sharp increase of hydraulic conductivity was expected, as the less decomposed sample will have less fine material to block flow, and therefore water can flow through the medium easily (Figure 2.4 [35]). A full overview of the results is given in the Appendix A.

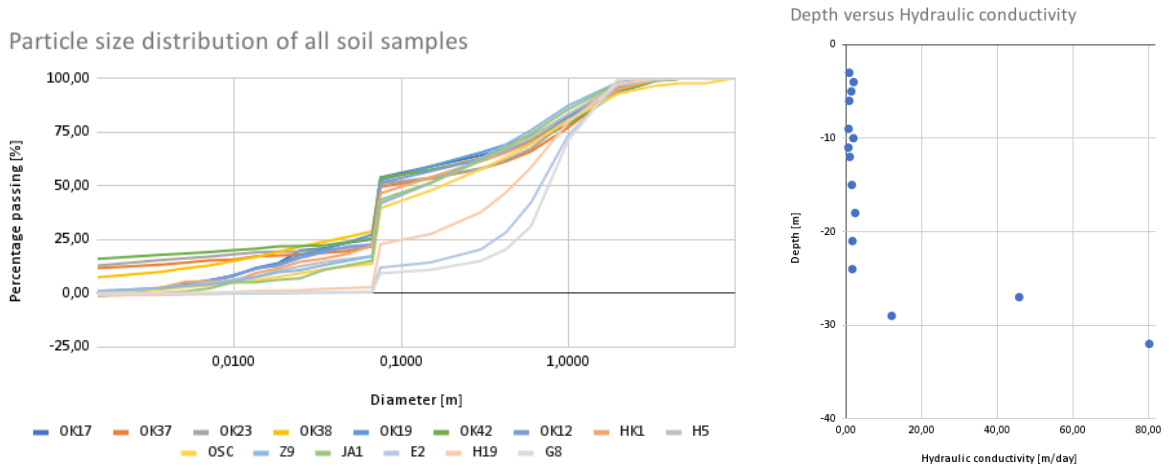

(a) The particle size distribution of all analyzed soil samples. The sharp drop in the middle of the section is caused by sample loss during washing after the hydrometer testing. The deeper samples show a less uniform distribution and are more coarse than the shallower samples.

(b) Calculated hydraulic conductivity with depth. A sharp increase is seen around 27 meters depth, close to where the water table is present.

Figure 4.5

4.2. MODFLOW 6 Models

4.2.1. Groundwater Level Response

All 5 MODFLOW 6 simulations show a clear response in hydraulic head level during precipitation events. The groundwater responds to rainfall in different aspects; the top layer (specific storage) responds faster and stronger than the bottom (phreatic storage), the infiltration of the rainwater changes over time for the MDP site, and seasonal trends are also driven by precipitation.

Infiltration Changes over Time

Several time steps were selected to show the different stages of groundwater level change from one rain event. In Figure 4.6 and 4.7 the top layer of the pilot and MDP site are shown respectively around a singular rain event. The left plot shows two hours before the rain event, the middle plot shows it during the rain event and the right plot shows it two hours after the rain event. The effect of precipitation is much more present in the MDP site than in the pilot site. Before the rain event, the groundwater level is generally low, and increases rapidly during the rainfall event, especially at the higher elevations. In the MDP site, this strong increase is always followed by a strong decrease in groundwater level at first, which slows down over time, just as observed in the time series of groundwater levels in the wells (Figure 4.2).

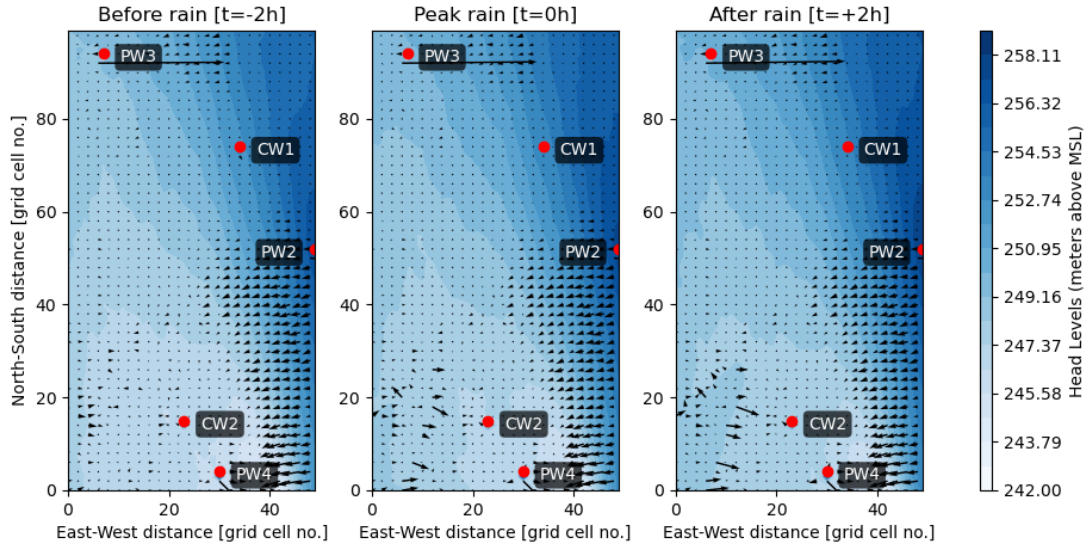

Figure 4.6: Pilot site top view of the top layer before, during, and after a singular rain event. The flow is pointed towards the lower elevation, and its magnitude increases during the rain event.

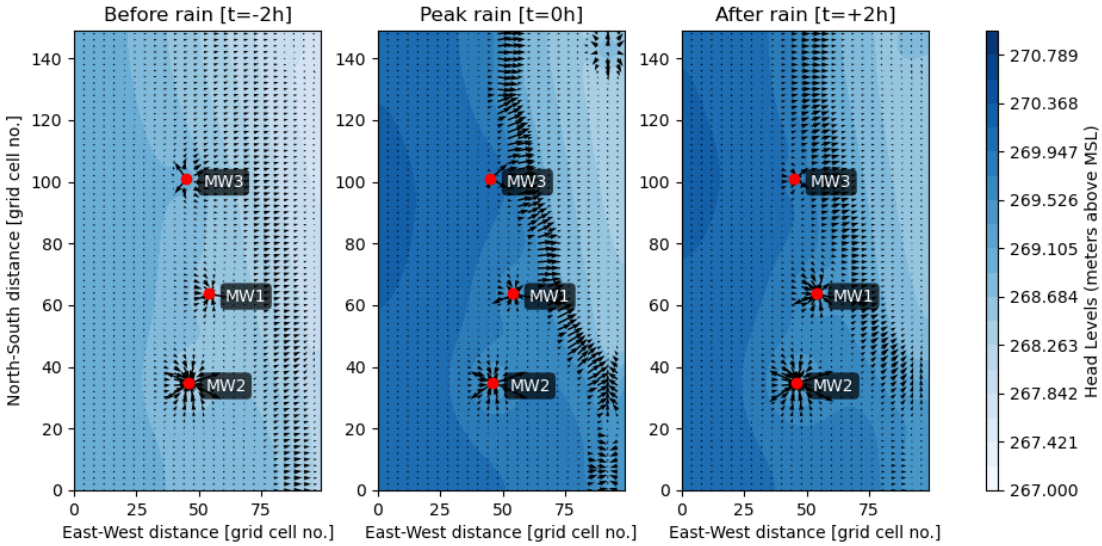

Figure 4.7: MDP site top view of the top layer before, during, and after a singular rain event. The flow is pointed towards the lower elevation, and its magnitude increases during the rain.

Over a time frame of two weeks (Figure 4.8 and 4.9), the slow response of the groundwater level in the pilot site is visible. The first period, around the 21st of September, was very dry, while the second and third period had significant amounts of rain. The MDP site shows an increase in groundwater level from the 28th of September onward, though the last period shows a similar groundwater level. The fast dissipation of groundwater dampens the longer term effects of precipitation. However, the groundwater level in the pilot site shows a continuous large increase in groundwater level over the two weeks. The low hydraulic conductivity attenuates dissipation outside of the modeled site, and therefore the groundwater level keeps increasing.

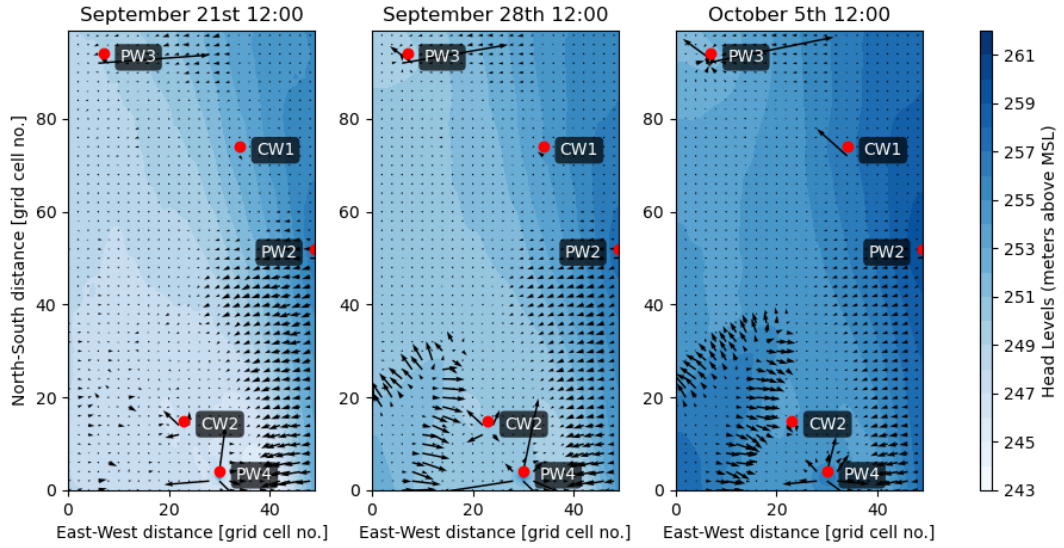

Figure 4.8: Pilot site top view of the top layer over 2 weeks. The flow is pointed towards the lower elevation.

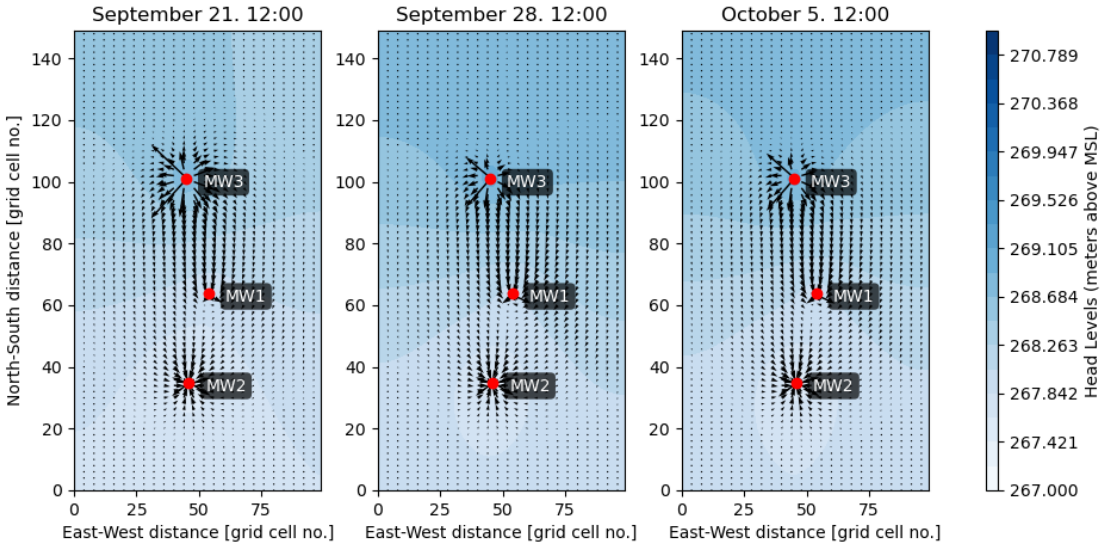

Figure 4.9: MDP site top view of the top layer over 2 weeks. The flow is pointed towards the lower elevation

Due to the low hydraulic conductivity present in the top layer of the pilot site, the response to rainfall is biased. The hydraulic head data includes the direct response via MAR of the hydraulic head level, though this is not via natural infiltration. The subsequent response to this is shown in Figure 4.10a and 4.10c. Once the volume in the upper layer is increased by MAR, the infiltration into the lower layers and to the sides is very slow compared to the MDP site (Figure 4.10b). In conclusion, the pilot site cannot be looked at for short term changes in the groundwater level, while the MDP site gives more insight in the natural response of groundwater level to precipitation.

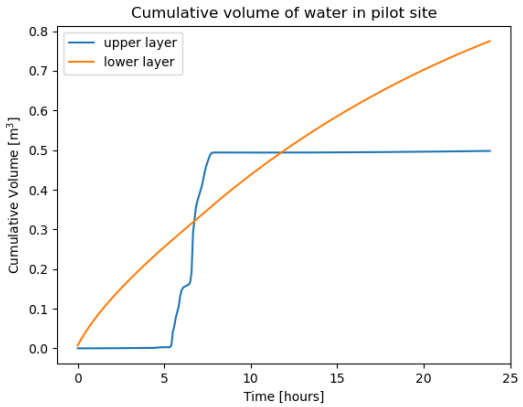

(a) Cumulative volume over the pilot site in one singular rain event. The upper layer shows a clear fast response to rainfall and the lower layer has an unnatural response due to input parameters.

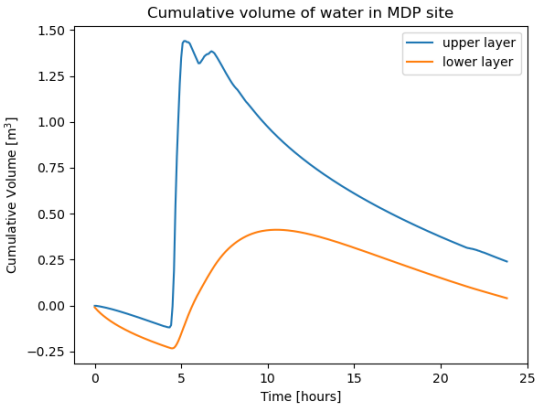

(b) Cumulative volume over the MDP site in one singular rain event. The lower layer has a delayed and dampened response to rainfall compared to the upper layer.

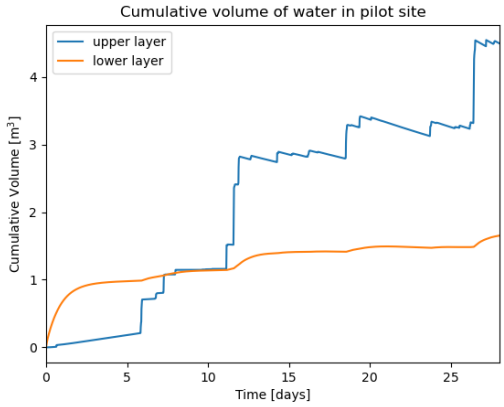

(c) Cumulative volume over the pilot site over 28 days. After ten days the lower layer shows a natural response to rainfall that is much smaller and more steady than the upper layer.

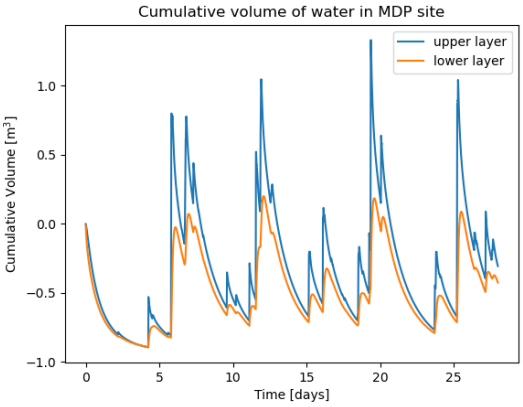

(d) Cumulative volume over the MDP site over 28 days. The lower layer has a direct, but dampened response to rainfall compared to the upper layer.

Figure 4.10: Cumulative water volumes over measurement area.

Seasonal Response to Rainfall

In addition to short-term responses to rainfall, the groundwater table is also seasonally dependent on precipitation. Though the model for the pilot site is lacking for the short time scales, the long data collection period gives room for long-term changes of the cumulative volume, which is empirical when dealing with low hydraulic conductivities. As seen in Figure 4.11, a general trend similar to the wet and dry seasons can be seen. Note that the boundaries of the fitted dataset are not looked at, as polynomial data fitting is not suitable for extrapolation and fitting of the boundaries. The first two peaks are related to the first and second wet season in June-July and September-October-November respectively. Then, a slight depletion in cumulative volume is seen in the dry season from December-March, after which the total volume increases again as the next rain season begins. It is clearly seen in the data that July and August of 2024 were relatively dry, as there is a net depletion again. This observation emphasizes the importance of recharge during wet periods, as longer dry seasons will lead to much more depletion year round.

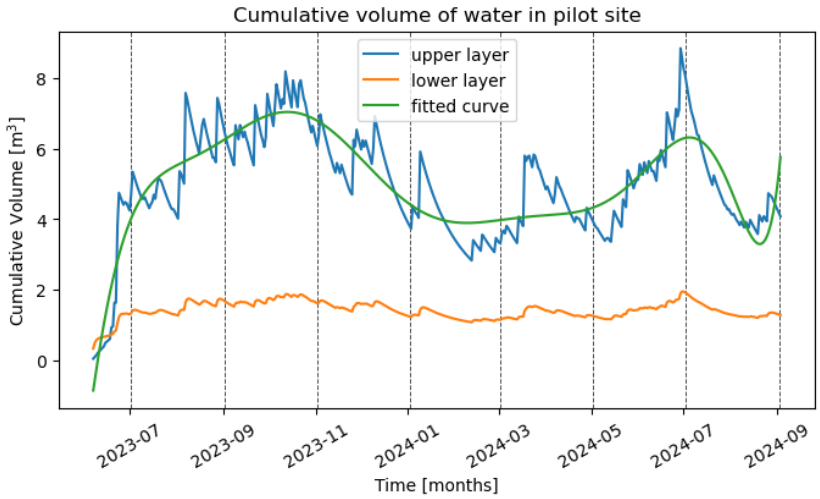

Figure 4.11: The monthly cumulative water volume of the entire pilot site. The fitted curve shows a trend that corresponds with the wet and dry seasons discussed in chapter 2.

Difference Specific and Phreatic Storage

The phreatic zone is the semi-permanent saturated zone in the shallow subsurface. The layer that often varies in saturation on top of the phreatic zone is where specific storage is present. We can state that the lower layer, which is below the boundary of the static hydraulic head, can be seen as the area optimal for phreatic storage, while the top layer holds specific storage.

The top layer of the surface shows a direct response to rainfall events, showing a rapid rise in hydraulic heads during the periods of precipitation and, in the MDP site, a fast drop following these events, due to dissipation outside the system and to the layer below. In contrast, the bottom layer is less influenced by rainfall, as it demonstrates a dampened and slightly delayed reaction. In the pilot site, however, the phreatic storage is changed as a result of the additional groundwater level increase caused by MAR, though it keeps increasing over time (Figure 4.10a). This is not the expected natural response and is therefore considered inaccurate. This bias is not present in the MDP site since there is no MAR and all changes in groundwater level are due to natural infiltration from the precipitation and runoff. The changes in surface elevation have similar influence on flow direction in both the top and bottom layer.

4.2.2. Influence of MAR on Groundwater Level

Figures 4.12 and 4.13 show the difference per time step in hydraulic head in the top layer for the pilot site and MDP site respectively. The left plot shows two hours before the rain event, the middle plot shows it during the rain event and the right plot shows it two hours after the rain event. For both sites, the hydraulic heads increase during the rain, after which the water level dissipation is different for each site. For the MDP site, the groundwater level decreases due to the rain infiltrating in the soil and flowing away, and two hours after the rain event the biggest difference is in the flow at lower elevation. This indicates further that the groundwater flows from higher to lower elevations (also seen in Figure 4.7). For the pilot site, however, there is almost no infiltration into the system, as the hydraulic conductivity is very low and therefore the infiltration rate is very low as well. Therefore, a timescale of two hours is too short.

Furthermore, it can be seen that for the pilot site the hydraulic head increases by about 4.5 mm for a rainfall event of 19.2 mm, while for the MDP site the hydraulic head increases by about 238.0 mm for a rainfall event of 33.5 mm. The latter increase is unexpected, as the change in hydraulic head is immensely higher than the recharge per squared meter. This is likely because the MDP site has a generally low elevation and a high hydraulic conductivity, and is therefore a waterlogged area. In other words, the precipitation of a far larger area around the MDP site is collected here. The increase in groundwater level in the pilot site is the result of the injection of MAR, as the natural infiltration in this area is not fast enough to have this immediate response.

Note that this observation can help in determining the locations of possible MAR points. In areas with a similar geology as the MDP site, wells can be further apart and can be located in high elevations only, due to the high hydraulic conductivity of the upper layer the wells at lower elevation will be recharged via fast flow from high to low elevation. However, in areas with a similar geology as the pilot site, wells utilizing MAR need to be relatively closer together and will need to be placed in areas with higher and lower surface elevation. This is because the flow through the upper layer is much slower and will have limited response shortly after the rain events.

It is important to note that this same reason highlights the demand for MAR in areas with low hydraulic conductivity over areas with high hydraulic conductivity. Natural infiltration from rain is much more limited in the former, so in order to store more water to use during dry seasons and the years to come, MAR is an effective tool to utilize the highly permeable lower layer. As shown in Figure 4.10a and 4.10c, individual rain events will not provide accurate representations of the MAR effect in layers with low hydraulic conductivity, though extensive measurement periods will give great insight on this (highlighted in Figure 4.11).

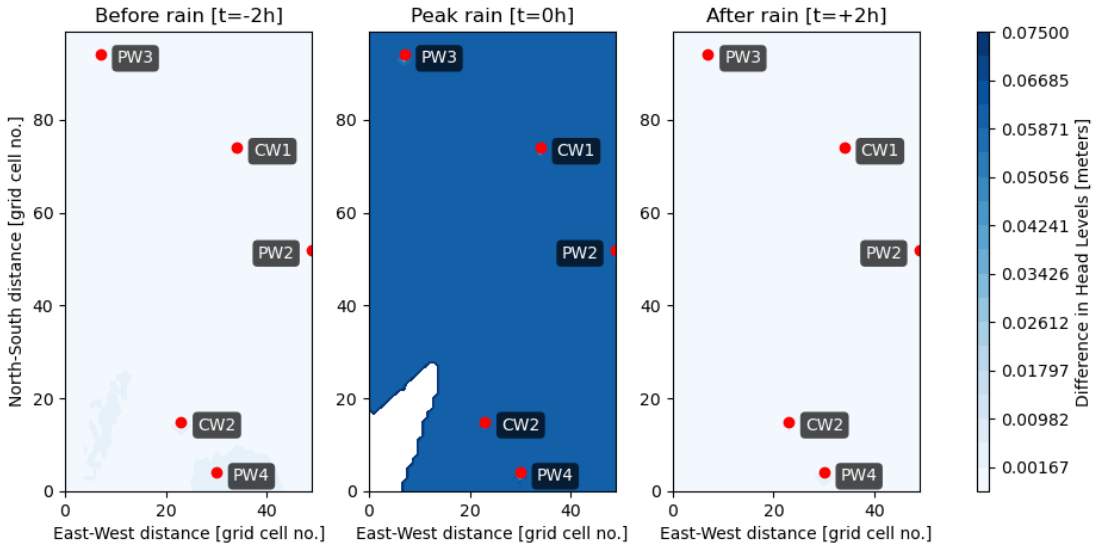

Figure 4.12: Difference in hydraulic heads in the top layer of the pilot site at three different time steps, before, during and after the rain event.

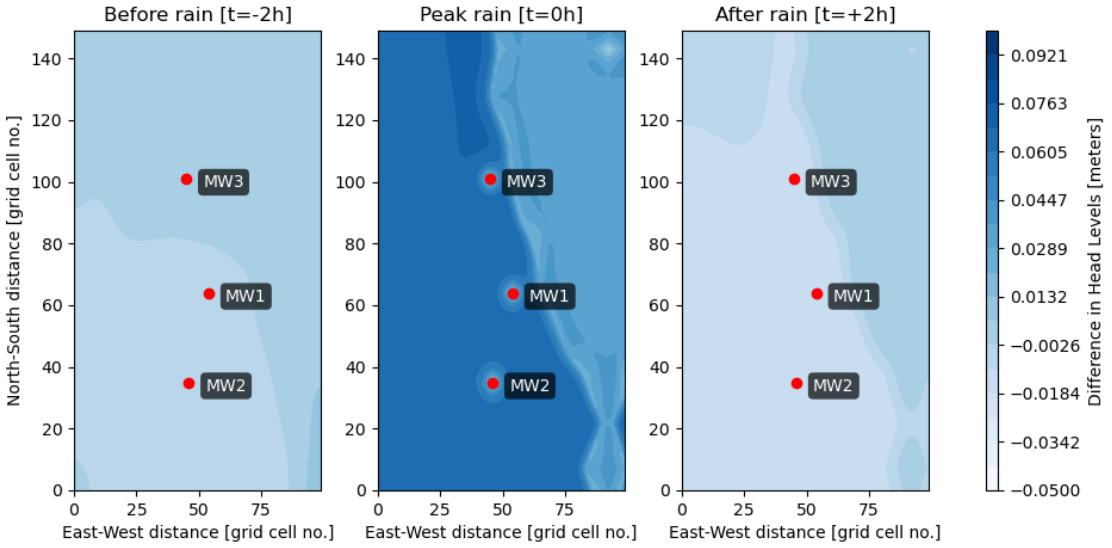

Figure 4.13: Difference in hydraulic heads in the top layer of the MDP site at three different time steps, before, during and after the rain event.

4.2.3. Quantitative Assessment of MAR

From the cumulative volumetric change in Figure 4.10 it can be seen that the groundwater volume in the upper layer follows an upward trend with an increase of 4.0 m^3 over the 28 days measuring period at the pilot site. In contrast, a decline of 0.3 m^3 in groundwater volume was observed at the MDP site for the same time period. It is assumed that this difference between the two sites is caused by the MAR systems which are present at the pilot site, but not at the MDP site, since similar amounts of rainfall was measured in both areas, 206 mm at the pilot site vs 266 mm at the MDP site. This assumption is the best estimate for the total influence of MAR that can be obtained from the short measuring period of 28 days, keeping in mind that the areas contain several different conditions such as the MDP site being waterlogged while the pilot site is not and the the difference in hydraulic conductivity.

By comparing the volumetric change over 28 days found over the sites with and without MAR, the volumetric effect of MAR on the yearly groundwater volume was obtained and extrapolated to the entire Kumasi Metropolitan Area following Equation 3.4 - 3.6. The yearly groundwater depletion estimate based on the input-output method from Potter [48] is 2.2 Mm^3 over Kumasi in total. When assuming an urban area of 254 km^2 for Kumasi and an average rooftop area of 105 m^2 per MAR system based on the pilot site, 2503 wells are needed to avoid further groundwater depletion under the current consumption and natural recharge over peri-urban Kumasi. This corresponds to one well connected to a MAR system per 1600 inhabitants.

This estimate seems reasonable if the artificial recharge is based entirely on these small-scale systems and no large MAR systems would be implemented.

4.3. Qualitative assessment of MODFLOW 6 Models

The MODFLOW 6 models assume the changes seen in hydraulic head are a result of changes in precipitation, phreatic storage, and specific storage. However, the increase seen in the wells is influenced by MAR, and therefore the interpolated hydraulic heads are highly exaggerated. As a result, the phreatic and specific storage are assumed to change significantly, which is not the case. Therefore, using this configuration of MODFLOW 6 is not suitable for modelling the effect of MAR on groundwater level.

In contrast to the MODFLOW 6 model, the 2D simulator – discussed in chapter 5 – uses changes in injection rate as a way to model changes in the groundwater level. Here, no changes in the storage of the system and no natural infiltration of the precipitation are assumed. This is conceptually more similar to the process of MAR, and it is therefore a better fit to model the effects of MAR on groundwater levels.

However, this model is severely limited, as it does not allow a change in volume and natural infiltration (only injection through wells), and is therefore also not suitable to model groundwater levels with MAR.

In MODFLOW 6, one can add separate wells instead of using the direct hydraulic head changes as input, where MAR can be modelled much better. However, then the natural infiltration is again not taken into account. Therefore, the optimal model configuration would entail differentiating the hydraulic head input into the natural effects of precipitation and the added effect of MAR. Then, this can be both included as direct hydraulic head data and well injection respectively, to give an accurate groundwater level model. Note that splitting the data is extremely difficult. However, using test sites with and without MAR can give an indication of the influence of MAR, as has been done in this report. Note that comparing similar sites in geology and surface elevation will give data sets that are more easily compared to each other.

5

Experimental Trial of 2D Simulator

To compare the 16 month results of the MODFLOW 6 model over the pilot site and determine whether this region is predominantly influenced by natural recharge or MAR, we developed a 2D-Simulator to focus exclusively on the effects of MAR. This is achieved by treating the wells as injectors and precipitation as the only inflow of the model, effectively removing the impact of natural recharge from the analysis. By isolating MAR's influence, the contribution of MAR on groundwater levels and flow patterns is better understood.

5.1. Model Construction

In this model setup, a single-phase, connection-based 2D simulator with wells is employed, utilizing the Finite Volume Method (FVM) with the Backward Euler scheme for time integration. The governing equation is derived from mass conservation principles:

$$\frac{\partial}{\partial t}(\phi\rho) - \nabla \cdot \rho\frac{K}{\mu}\nabla p = -\tilde{m} \tag{5.1}$$

- ϕ is the porosity [-];
- ρ is the fluid density [kg/m^3];
- μ is the viscosity [Pa s];
- K is the hydraulic conductivity [m/day];
- p is the pressure of the hydraulic head [Pa];
- $\tilde{m}$ is the source term [kg].

The model incorporates detailed well dynamics, such as injection rates and well inflow performance, which influence fluid flow near the well. To simulate MAR systems, injection wells are positioned at the locations of existing MAR wells, imposing time-varying pressure changes based on observed groundwater level fluctuations.

Given the uncertainty regarding the exact boundary conditions, the injection rates of the wells in the model are designed to represent the net effect of MAR —specifically, the balance between MAR infiltration and depletion. The infiltration attributed to MAR is estimated by subtracting the infiltration rates of wells not equipped with MAR systems from those that are equipped with MAR systems. This approach justifies treating the boundaries as zero-flux surfaces while allowing the wells to function solely as injectors. By isolating the system in this way, we simplify the boundary conditions while still effectively offsetting the influence of natural recharge and focusing the model on capturing the dynamics of MAR alone.

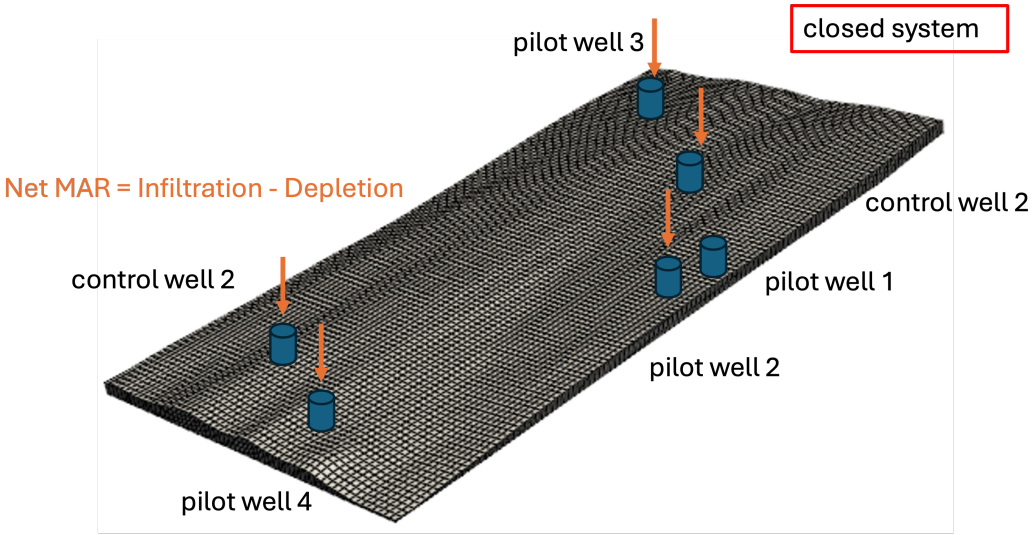

Figure 5.1: Visualization of pilot site model with well injectors.

The static mean groundwater level, derived using co-kriging, serves as the initial condition for the model. The initial pressure distribution is then computed by incorporating the effects of gravity, ensuring that the model accurately reflects the hydrostatic conditions in the subsurface. This approach ensures that the pressure field is consistent with the spatial variations in groundwater elevation, which is critical for accurate simulation of groundwater flow and hydraulic processes.

Even though water is treated as incompressible, implying a constant density, the soil analysis indicates that the medium consists of sandy loam material. This suggests that porosity changes over time, $\frac{d\phi}{dt}$, may not be negligible, particularly in regions with significant pressure variations. In such cases, the compressibility of the soil becomes an important factor. For example, in silty soils, a pressure gradient ranging from 1,000 to 10,000 Pa/m can lead to noticeable structural changes within the soil matrix, thereby affecting its porosity. As shown in Figure 5.2, there is a marked pressure transient zone on the right side of the plot where the pressure gradient exceeds 1,000 Pa/m. This steep gradient could induce non-negligible changes in the soil structure, leading to dynamic variations in porosity. Given this scenario, it is essential to incorporate a compressible simulation model. Such a model would more accurately reflect the evolving nature of the subsurface system, accounting for changes in soil compressibility due to pressure variations. This adjustment is necessary to capture the realistic behavior of the system, especially in regions experiencing abrupt pressure changes, where porosity and structural deformation may significantly impact fluid flow.

This 2D model focuses on simulating the hydraulic head level, utilizing a connection based approach that specifically tracks flow through the interfaces between grids. To calculate the area of each interface in an unstructured grid system, the variable grid thickness (δz) is required for each grid cell. The model assumes uniform porosity and hydraulic conductivity across the hydraulic head layer, based on soil analysis.

As the simulation progresses through multiple time steps, changes in groundwater levels can be observed from a top-down perspective, reflecting the dynamic behavior of the system. Although pressure is the primary output, it can be converted into water levels by factoring out the effects of gravity—this involves accounting for fluid density, gravitational acceleration, and the assumed porosity of the medium. This conversion allows for a more intuitive interpretation of the model output in terms of groundwater levels, making it easier to assess aquifer dynamics over time.

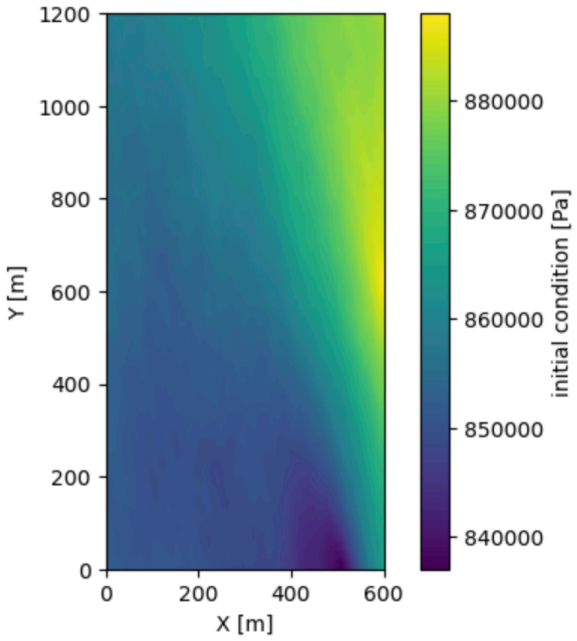

Figure 5.2: Pressure distribution over the pilot site groundwater in the initial model state.

5.2. Result Display

The simulator faced constraints related to computational time, necessitating the use of a 2D model rather than a 3D representation. Consequently, this led to a simplification of the system, particularly in the characterization of the unsaturated zone, which may have impacted the accuracy of the model. As demonstrated in Figure 5.3, the hydraulic head differences between time steps were unreasonably large. The fake uniform/even groundwater level derived from the equations might be caused by the minimal variation in the initial hydraulic head in the wells. This limited variation can lead to an excessively large hydraulic gradient, preventing proper flow simulation. Another potential issue could be the “closed” boundary conditions, which restrict the exchange of water across the boundaries, effectively isolating the system. Therefore, the results of the model cannot be used. However, a qualitative analysis between the MODFLOW 6 model and the 2D simulator is done in section 4.3

Based on observed infiltration and depletion rates, the net MAR rate is time-dependent. After approximately 10 hours, the net MAR rate approaches zero. Consequently, the model’s time span is constrained to 12 hours to capture the relevant dynamics within this period.

5.3. Validity and Deficiencies of the Simulator

The Compressible 2D Single Phase Simulator, originally designed for reservoir modeling applications in areas such as Carbon Capture and Storage (CCS), can potentially be adapted for hydrogeological modelling with appropriate modification. Given the underlying similarities in the physical processes involved, it is worthwhile to assess its validity for this new application.

The core principles of fluid flow in porous media, such as mass conservation law, Darcy’s law and the continuity equation, govern both CCS and hydraulic systems. In CCS, the objective is to model the movement and storage of CO_2 in subsurface reservoirs, while in hydraulic modelling, the focus is on groundwater movement. In both cases, pressure gradients are the key drivers of fluid flow. The pressure perturbations caused by injection wells affect fluid flow near the well, a phenomenon closely analogous to CO_2 injection in CCS [24]. This similarity underscores the feasibility of a reservoir framework to hydraulic modelling, particularly when investigating groundwater flow, infiltration, or recharge dynamics.

While the fundamental principles of the model are sound, several key areas require improvement to

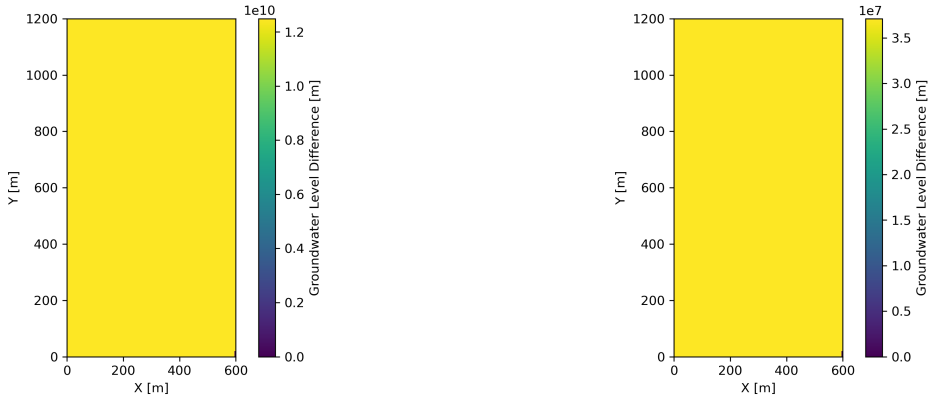

(a) 2D ground water level change after 2 hours

(b) 2D ground water level change after 12 hours

Figure 5.3: Change in groundwater level with different time steps obtained from the 2D simulator over the pilot site. It can be seen that the change is huge over the whole site, which is not feasible in reality.

enhance its accuracy and applicability:

- **Boundary Conditions:** In hydraulic modelling, the boundary conditions often need to account for the unsaturated zone, which adds complexity when modeling groundwater systems. Modifying boundary conditions to accurately represent interactions between saturated and unsaturated zones can be particularly challenging. This highlights the potential of the 2D simulator for future enhancements. By incorporating more sophisticated boundary conditions, the model could significantly improve simulation precision, especially in distinguishing between natural recharge and MAR dominant areas. These improvements would result in a more reliable assessment of MAR interventions and the natural recharge dynamics, leading to better water resource management strategies.
- Figure 4.8 and 4.9 In reservoir modelling, particularly in CCS or Carbon Capture, Utilization, and Storage (CCUS), two-phase flow models, e.g. water and oil replaced by CO_2, are often employed. However, in typical hydraulic models, fluid behavior is simplified to a single phase (water), which may overlook critical dynamics. For accurate hydraulic modeling, air should be considered as a second phase, alongside water. Simplifying the system by ignoring residuals in the unsaturated zone or the replacement processes introduces unpredictability in water flow, aquifer dynamics, and pressure distribution. Properly modeling these interactions is essential to mitigate risks and improve the accuracy of predictions, particularly in regions where the unsaturated zone plays a significant role in groundwater behavior [50].

With these modifications, a reservoir modeling framework could feasibly be adapted for hydraulic systems, offering valuable insights into aquifer dynamics, infiltration processes, and flow patterns. However, further investigation and development are necessary to address the current deficiencies, particularly in boundary condition handling and multi-phase fluid representation, before such an adaptation can be fully realized.

6

Discussion

6.1. Uncertainties and Errors in Data Gathering

One of the biggest challenges of this project was clearly the limited data availability. Simultaneously, this emphasizes the importance of such studies, that aim to improve the available knowledge about groundwater in this region. The errors associated with limited data are presented as follows:

- **Long Data Gaps:** In the pilot project, three out of six wells experienced major data gaps during the one-year data record, which is already considered as a short time frame for groundwater observation. Out of this period, the diver in pilot well 1 was broken for an extended amount of time, leaving only one month of reliable data. At pilot well 2 and control well 1, reliable data was only available from 2023 and August-September 2024, presenting challenges for modelling over a full year time period. Hence, the most reliable results of our analysis come from pilot well 3 and 4, as well as control well 2, which have a continuous data record with very few and small data gaps.
- **Changes in Rope Length:** The rope length, at which the diver is suspended in the well, has been changed multiple times during the one year period at pilot well 2 and control well 1, to keep the diver in the water without extending its measuring range of ten meters. This is noticeable in the unnatural looking jumps in the water level data. However, since the timing and change in length were not recorded, the data could not be corrected appropriately. This problem only affects the monthly average water level used in the 16 month model.
- **Submerged Barometer:** At the MDP site, the barometer was submerged in water for one day due to a heavy rainfall event. To address this issue, the barometric data from the nearby pilot site was used in order to correct the MDP diver data. This approach is supported by the vanEssen diver manual, which states that barometric compensation is valid for distances up to 15 km, and the two sites fall within 15 km of each other. To validate this substitution, a comparison was made between barometric measurements from both sites over other time periods. Other than a slight offset, the barometric trends were very similar. Consequently, this offset was adjusted for to ensure compatibility, before applying the pilot site's barometric data to correct the MDP diver data.
- **Missing Five Minute Pressure Data:** At the start of the 28 days data acquisition period, all divers were set to measure in five minute intervals. However, the pilot barometer was not updated accordingly. As a result, the hourly barometric data was used to compensate the diver measurements collected every five minutes during this specific time period.
- **Diver Not Submerged:** Errors are primarily caused by measurements taken when the diver was not submerged in water. This can be due to low groundwater levels or because the diver was taken out of the water when retrieving data or water is collected from the well.

6.2. Data Processing and Assumptions

In this report, it was assumed that groundwater level and precipitation are linearly related. However, groundwater flow complicates this matter. The results clearly indicate that deeper wells react very different to precipitation events compared to shallow wells, with the well elevation also having an impact on this response. Although daily water level and precipitation correlations provide validation for relation between groundwater level and precipitation, it leads to loss of information from single precipitation events. Because infiltration with MAR changes on short timescales, this approach is not recommended for estimating the immediate effects of MAR on the groundwater level.

Additionally, groundwater extraction by local users was not completely accounted for and evapotranspiration was not taken into consideration, which introduced significant uncertainty and inconsistency in the correlation results. This omission particularly complicated the comparison of groundwater volumetric changes between wells with and without MAR at the pilot site. Due to this missing assumption regarding extraction, the models were constructed with inherent limitations, leading to less reliable predictions of groundwater dynamics and MAR's impact. Future models should incorporate data on human extraction to improve the accuracy of volumetric change estimates and allow for a more precise evaluation of MAR's effectiveness.

6.3. Uncertainty Quantification in Geo-Modelling

6.3.1. Vertical and Horizontal Heterogeneity

- The spatial distribution of facies associations across the entire computed domain is not well-constrained due to limited data availability. Instead of capturing the actual variability, a single vertical hydraulic conductivity value for each section of saprolite, has been extrapolated and uniformly applied across the entire model domain. While this simplification is often necessary due to data scarcity, it may not accurately reflect the inherent heterogeneity in the subsurface environment. Such oversimplification can lead to inaccuracies in predicting subsurface flow behavior and resource distribution.
- The thickness of the aquifer, a critical parameter for assessing groundwater storage and flow dynamics, is also poorly constrained due to a lack of detailed data. In the absence of direct measurements or detailed geological characterization, a uniform aquifer thickness has been assumed across the model region. This assumption does not account for potential variability in aquifer geometry, which can significantly affect flow and transport processes. Consequently, this generalization introduces a significant source of uncertainty in the overall hydrological and geological model.

6.3.2. Data Interpolation

The limited availability of hydraulic head presents a major challenge in the modelling process. Due to the scarcity of data points, particularly in subsurface environments, interpolation techniques are employed to estimate values across unsampled areas. However, the sparse distribution of data leads to several issues:

- **Risk of Overfitting:** With limited data points available, there is a high risk that the model may overfit the existing data. In such cases, the model is tuned too closely to the available data, potentially capturing noise or anomalies rather than underlying trends. As a result, the model may perform well in regions close to the data points but provide unrealistic or overly confident predictions in areas far from them.
- **Assumptions in Interpolated Zones:** In regions where the data is absent, the model's reliance on interpolation introduces uncertainty, especially if the interpolated values are based on simplistic assumptions of spatial continuity. For example, geological properties such as hydraulic conductivity may vary significantly even over short distances due to lithological changes, and these variations may not be adequately captured by the interpolation process. This could lead to unrealistic or erroneous predictions of groundwater flow, storage, and other subsurface processes.

6.3.3. Hydraulic Conductivity Derived from Empirical Relations

The estimation of key subsurface parameters such as hydraulic conductivity is another area of uncertainty in the model. In this case, direct measurements of hydraulic conductivity were not available; instead, these properties were inferred through semi-empirical relationships based on the particle size distribution of soil samples:

- **Empirical Estimations:** The particle size distribution, which can be determined through sieving or sedimentation tests, is often used to approximate hydraulic conductivity using established empirical formulas. While this method is practical and widely used in the absence of more precise measurements, it introduces uncertainty because these relationships are not always universally applicable. The actual relationship can vary based on local geological conditions, such as particle shape, lithology or the void ratio.
- **Uncertainty in Spatial Variation:** Additionally, the relationship between these parameters may change across the region due to differences in e.g. lithology and post-depositional processes. For example, hydraulic conductivity can vary significantly even within a single lithologic unit due to factors like fractures, faulting, or varying degrees of sorting. These variations are not accounted for in the model, as it assumes a consistent relationship between particle size and hydraulic conductivity throughout the entire domain.

In summary, while empirical relationships provide useful means for estimating subsurface properties, the inherent uncertainty in these approximations, combined with the lack of direct measurements, can lead to significant errors in model predictions. These errors are compounded by the fact that the spatial variability of hydraulic conductivity is not fully represented, potentially resulting in inaccurate simulations of subsurface processes.

7

Conclusion

This study aims to improve the monitoring of groundwater dynamics in Kumasi with regard to the contribution of MAR, by conducting groundwater level measurements in sites with and without MAR. Dynamic groundwater models have been developed which provide insight into groundwater flow and the response of groundwater to precipitation.

The analysis showed a correlation between the daily amount of groundwater level increase and precipitation, particularly in wells with MAR systems, indicating that the MAR significantly increases the groundwater recharge from precipitation. The groundwater level is often located around the base of the saprolite, where the overburden is slightly coarser and has a higher hydraulic conductivity. However, in waterlogged areas, the water level is significantly shallower than this.

Due to the high hydraulic conductivity in the upper layer of the waterlogged site without MAR, the groundwater level increases fast during a rain event, and dissipates very fast towards the lowest elevations afterwards. Therefore, in similar areas, MAR should be implemented in high elevations only and the distance between wells using MAR can be quite large.

Due to the low hydraulic conductivity of the upper layer in the area with MAR, the groundwater level increases fast during a rain event by injection through MAR, but the water does not flow quickly to the lower elevations. The response is only seen after weeks, and seasonal variations can be seen in this type of medium as well. Natural infiltration of the precipitation is very limited towards the lower, more permeable layer. Therefore, MAR is much more effective and needed in these areas if more water is to be stored long-term. Note that more wells using MAR should be installed in this geology, where the wells are installed closer together and in areas with both high and low surface elevation.

The difference in groundwater volume over 28 days in the wet period varied notably between the site with and without MAR. At the site without MAR, groundwater depletion amounted to -0.3 m^3 over 28 days while the site with MAR experienced an increase of 4.0 m^3, showing the positive influence of MAR on groundwater recharge. Nevertheless, these values are extremely small compared to the research area.

Though the volumetric change in groundwater is minimal, it was used to quantify the number of MAR systems needed to avoid groundwater depletion in the whole peri-urban area of Kumasi. It was found that for an average rooftop area of 105 m^2 per MAR system, around one well with MAR for every 1600 inhabitants is needed to avoid groundwater depletion in Kumasi. However, this value should be critically evaluated and additional quantitative research must be done.

These results are limited by the short data record and sparse data availability of groundwater and soil data in Kumasi. Other limitations concern the model assumptions, input parameters, and the incorporation of MAR in groundwater models. Extended data collection and aiming to differentiate hydraulic head data into the natural infiltration and the effect of MAR is strongly recommended for solving the issue of groundwater sustainability in Kumasi.

8

Recommendations

The recommendations resulting from this research can be divided into two categories: recommendations on the extension of the actual research, and general recommendations on the issue regarding the rapid groundwater depletion in and around Kumasi.

Extension of the Research

This research has focused on modelling groundwater levels in small scale research areas, using different time frames. However, the report does not find a reproducible relation between the elevation, geology, and water levels, which could support the extrapolation in a model over the entire Kumasi area. This is therefore recommended as further research.

If more measurement equipment and time is available, one should compare the data obtained in this report with newly obtained data in different sections of Kumasi. Then, an extensive monitoring network will aid in identifying the diversity of groundwater flow throughout Kumasi and in selecting suitable locations for MAR.

When performing a suitability analysis on where new MAR systems should be implemented, one should consider water logged areas and low elevation areas as unsuitable. Areas with low hydraulic conductivity in the upper layer, high elevation or a lot of extraction have a higher risk of groundwater scarcity, which is why MAR applications in these areas are desirable. Furthermore, the recommended number of wells to be used for MAR to combat groundwater depletion does not take well capacity, the distance between MAR wells, or population and consumption increases into account. This should therefore also be investigated when considering the potential of MAR alone to halt the groundwater depletion rates.

The model itself also has limitations that can be improved. The hydraulic head should be discretized into changes in natural infiltration and groundwater flow, and the additions caused by MAR and extraction. Then, this can be divided in the models, and the true effect of MAR can be analyzed. Furthermore, more detailed geologic maps, including in-situ hydraulic conductivity tests and structure of the layers, will give more insight in the flow paths the groundwater will tend to take.

Combating Groundwater Depletion

When performing groundwater level measurements or MAR installation in private wells, the support and consent of the owners is very important for the success of the project, since they have to make sure to keep the divers safe and put the divers back in the wells every time after collecting water. Therefore, a close connection with the community is a vital first step to combat rapid groundwater depletion. This can be achieved by talking to, listening to, and informing the population of the issue and their role in the solution.

Additionally, the rooftop area connected to each MAR system should be considered, since larger rooftop areas e.g. on commercial buildings, would lower the necessary amount of wells. However the distribution of artificial recharge also plays a key role in avoiding groundwater depletion. A suggestion is

therefore to urge high consumption companies to implement larger scale MAR systems close to their extraction sites.

Furthermore, an extensive database of active wells needs to be established so that a detailed estimate can be made regarding the groundwater extraction. Perhaps the most challenging part in this will be estimating the groundwater depletion caused by (large) companies. This is often done without (drilling) permits or strong regulations in terms of amount of water they can extract. Therefore, strong and upheld regulations are advised, where a community vigilance is needed to ensure no illegal drilling and over-extraction occurs. This circles back to the strong sense of trust and connection that is needed with the community.

References

[1] Abass, K., Adanu, S. K., and Agyemang, S., "Peri-urbanisation and loss of arable land in kumasi metropolis in three decades: Evidence from remote sensing image analysis," *Land Use Policy*, vol. 72, pp. 470–479, 2018, ISSN: 0264-8377. DOI: https://doi.org/10.1016/j.landusepol.2018.01.013. [Online]. Available: https://www.sciencedirect.com/science/article/pii/S0264837717301746.

[2] Abija, F. A., "Predicting aquifer storage properties integrating geoeletric methods with dynamically derived geomechanical parameters in parts of cross river state, nigeria," *American Journal of Water Science and Engineering*, vol. 9, no. 2, pp. 174–183, 2020.

[3] Afrifa, B. B., "The lithology and soil geochemistry of ntumkumso and its surrounding areas in the ashanti region of ghana," Ph.D. dissertation, University of Ghana, 2014.

[4] Almeida, A. P., Liberalesso, T., Silva, C. M., and Sousa, V., "Combining green roofs and rainwater harvesting systems in university buildings under different climate conditions," *Science of The Total Environment*, vol. 887, p. 163 719, 2023, ISSN: 0048-9697. DOI: https://doi.org/10.1016/j.scitotenv.2023.163719. [Online]. Available: https://www.sciencedirect.com/science/article/pii/S0048969723023409.

[5] Atta, S. K., "Mapping subsurface geological structures in the birimian supergroup, ghana using airborne magnetic and radiometric data: Implications for gold exploration," *Journal of African Earth Sciences*, vol. 205, p. 105 003, 2023.

[6] Ayetey, J. and Frempong, E., "Cartographie géotechnique en terrains tropicaux: L'expérience du ghana," *Bulletin of the International Association of Engineering Geology-Bulletin de l'Association Internationale de Géologie de l'Ingénieur*, vol. 54, pp. 33–43, 1996.

[7] Bagarello, V., Sferlazza, S., and Sgroi, A., "Testing laboratory methods to determine the anisotropy of saturated hydraulic conductivity in a sandy–loam soil," *Geoderma*, vol. 154, no. 1, pp. 52–58, 2009, ISSN: 0016-7061. DOI: https://doi.org/10.1016/j.geoderma.2009.09.012. [Online]. Available: https://www.sciencedirect.com/science/article/pii/S0016706109003115.

[8] Bakobie, N., Essandoh, H. M., Oduro-Kwarteng, S., Appiah-Adjei, E. K., Ahammad, S. Z., and Chakma, S., "Self-supply groundwater in five communities: Moshie zongo, aboabo, kotei, ayeduase and apemso in kumasi metropolis, ghana," *Heliyon*, vol. 10, no. 1, e23823, 2024, ISSN: 2405-8440. DOI: https://doi.org/10.1016/j.heliyon.2023.e23823. [Online]. Available: https://www.sciencedirect.com/science/article/pii/S2405844023110310.

[9] Bloem, M., "Urban mar," 2023, Thesis Report, TU Delft.

[10] Brown, C. E., *Applied multivariate statistics in geohydrology and related sciences*. Springer Science & Business Media, 2012.

[11] Cai, Y., Yin, Y., Kuang, X., Hao, Y., Liu, J., and Zheng, C., "Specific storage in aquitards," *Hydrogeology Journal*, vol. 31, no. 8, pp. 1999–2019, 2023.

[12] Carrier III, W. D., "Goodbye, hazen; hello, kozeny-carman," *Journal of geotechnical and geoenvironmental engineering*, vol. 129, no. 11, pp. 1054–1056, 2003.

[13] Chudasama, B., Porwal, A., Kreuzer, O. P., and Butera, K., "Geology, geodynamics and orogenic gold prospectivity modelling of the paleoproterozoic kumasi basin, ghana, west africa," *Ore Geology Reviews*, vol. 78, pp. 692–711, 2016.

[14] Chung, J.-w. and Rogers, J. D., "Interpolations of groundwater table elevation in dissected uplands," *Groundwater*, vol. 50, no. 4, pp. 598–607, 2012.

[15] Cities4Forests. "Kumasi." (2024), [Online]. Available: https://cities4forests.com/city/kumasi/ (visited on 10/03/2024).

[16] Columbia University, *Kumasi: Maps and population data*, Retrieved September 16, 2024, 2024. [Online]. Available: http://mci.ei.columbia.edu/millennium-cities/kumasi-ghana/kumasi-maps-and-population-data/.

[17] David P. Johnson, J., *Kumasi, Ghana*. Oxford University Press, 2010, p. 21, ISBN: 9780199733903. DOI: 10.1093/acref/9780195337709.013.2259. [Online]. Available: https://www.oxfordreference.com/view/10.1093/acref/9780195337709.001.0001/acref-9780195337709-e-2259.

[18] Digital Earth Africa and European Space Agency. "Copernicus digital elevation model (30 m)." (2024), [Online]. Available: https://maps.digitalearth.africa/ (visited on 09/22/2024).

[19] Dillon, P., Alley, W., Zheng, Y., *et al.*, *Managed aquifer recharge: Overview and governance*, IAH Special Publication, June 18, 2022, 2022. [Online]. Available: https://recharge.iah.org/files/2022/06/MAR-overview-and-governance-IAH-Special-Publication-18June2022.pdf.

[20] Donkor Ankrah Stephen Appiah Takyi, S. B. L. and Amponsah, O., "Urban sprawl, urban form, and urban land use pattern: Examining urban planning response to the causes and effects of urban sprawl in kumasi, ghana," *African Geographical Review*, vol. 0, no. 0, pp. 1–15, 2024. DOI: 10.1080/19376812.2024.2391777.

[21] Eisenlohr, B. and Hirdes, W., "The structural development of the early proterozoic birimian and tarkwaian rocks of southwest ghana, west africa," *Journal of African Earth Sciences (and the Middle East)*, vol. 14, no. 3, pp. 313–325, 1992.

[22] Ekeeda, *Hydrometer method of analysis - classification of soils - geotechnical engineering 1*. [Online]. Available: https://www.youtube.com/watch?v=Wx_eVuTdO4I.

[23] Ewusi, A., Asante-Annor, A., Seidu, J., and Fosu-Gyeabour, L., "Groundwater vulnerability assessment using drastic index and gis in kumasi metropolitan assembly, ghana," *Ghana Mining Journal*, vol. 16, no. 1, pp. 21–30, 2016.

[24] Fenske J.P. Leake S. A., P. D. E., "Simulating reservoir leakage in ground-water models," *Ground Water*, 1997.

[25] Feybesse, J.-L., Billa, M., Guerrot, C., *et al.*, "The paleoproterozoic ghanaian province: Geodynamic model and ore controls, including regional stress modeling," *Precambrian Research*, vol. 149, no. 3-4, pp. 149–196, 2006.

[26] Frimpong, B. F., Koranteng, A., Atta-Darkwa, T., Junior, O. F., and Zawiła-Niedźwiecki, T., "Land cover changes utilising landsat satellite imageries for the kumasi metropolis and its adjoining municipalities in ghana (1986–2022)," *Sensors*, vol. 23, no. 5, 2023, ISSN: 1424-8220. DOI: 10.3390/s23052644. [Online]. Available: https://www.mdpi.com/1424-8220/23/5/2644.

[27] Frimpong, B. F. and Molkenthin, F., "Tracking urban expansion using random forests for the classification of landsat imagery (1986–2015) and predicting urban/built-up areas for 2025: A study of the kumasi metropolis, ghana," *Land*, vol. 10, no. 1, 2021, ISSN: 2073-445X. DOI: 10.3390/land10010044. [Online]. Available: https://www.mdpi.com/2073-445X/10/1/44.

[28] Geleijnse, J., "Survey of water comsumption in kumasi," By courtesy of Jan Geleijnse and Edo Abraham, 2022.

[29] Ghana Statistical Service, Ministry of Finance, *2021 population and housing census - study documentation*, Oct. 2022.

[30] Google Earth Pro, *Kumasi, ashanti region, ghana*, Software, version 7.3.6.9796, Oct. 2024.

[31] Hirdes, W., Davis, D., Lüdtke, G., and Konan, G., "Two generations of birimian (paleoproterozoic) volcanic belts in northeastern côte d'ivoire (west africa): Consequences for the 'birimian controversy'," *Precambrian Research*, vol. 80, no. 3-4, pp. 173–191, 1996.

[32] Jan, C.-D., Chen, T.-H., and Lo, W.-C., "Effect of rainfall intensity and distribution on groundwater level fluctuations," *Journal of hydrology*, vol. 332, no. 3-4, pp. 348–360, 2007.

[33] Jessell, M. W., Amponsah, P. O., Baratoux, L., Asiedu, D. K., Loh, G. K., and Ganne, J., "Crustal-scale transcurrent shearing in the paleoproterozoic sefwi-sunyani-comoe region, west africa," *Precambrian Research*, vol. 212, pp. 155–168, 2012.

[34] Jing, X., Zhang, S., Zhang, J., Wang, Y., and Wang, Y., "Assessing efficiency and economic viability of rainwater harvesting systems for meeting non-potable water demands in four climatic zones of china," *Resources, Conservation and Recycling*, vol. 126, pp. 74–85, 2017, ISSN: 0921-3449. DOI: https://doi.org/10.1016/j.resconrec.2017.07.027. [Online]. Available: https://www.sciencedirect.com/science/article/pii/S0921344917302069.

[35] Jones, M. J., "The weathered zone aquifers of the basement complex areas of africa," *Quarterly Journal of Engineering Geology and Hydrogeology*, vol. 18, no. 1, pp. 35–46, 1985.

[36] Kesse, G. O., *The mineral and Rock Resources of Ghana*. A.A. Balkema; Distributed in USA & Canada by A.A. Balkema Publishers, 1985.

[37] Ketu, J. A., *Assessing the impact of future rainfall and urban growth on flood hazard in kumasi,ghana: Identifying potential flood mitigation measures.* Jul. 2024. [Online]. Available: http://essay.utwente.nl/100585/.

[38] Lenntech. "Water conductivity." (2024), [Online]. Available: https://www.lenntech.com/applications/ultrapure/conductivity/water-conductivity.htm (visited on 09/20/2024).

[39] Leube, A., Hirdes, W., Mauer, R., and Kesse, G. O., "The early proterozoic birimian supergroup of ghana and some aspects of its associated gold mineralization," *Precambrian research*, vol. 46, no. 1-2, pp. 139–165, 1990.

[40] Long, L. E., Castellana, C. H., and Sial, A. N., "Age, origin and cooling history of the coronel joão sá pluton, bahia, brazil," *Journal of Petrology*, vol. 46, no. 2, pp. 255–273, 2005.

[41] Manu, E., "Hydrogeochemical characterization of water resources in the pra basin (ghana) for quality assessment and water management: Field observations and geochemical modelling," Ph.D. dissertation, Universität Potsdam, 2023.

[42] McKenzie, A., Rutter, H., and Hulbert, A., "The use of elevation models to predict areas at risk of groundwater flooding," *Geological Society, London, Special Publications*, vol. 345, no. 1, pp. 75–79, 2010.

[43] Missoum, H., Belkhatir, M., and Bendani, K., "Undrained shear strength response under monotonic loading of chlef (algeria) sandy soil," *Arabian Journal of Geosciences*, vol. 6, Mar. 2011. DOI: 10.1007/s12517-011-0387-3.

[44] Nyako, S. O., Ofosu, B., Opuni, K., and Mensah, F. A., "Correlation between geological logs and geophysical logs to estimate aquifer positions in the crystalline basement rocks of the birimian system, ghana," 2016.

[45] Ofori, J., *Kumasi faces water crisis as gwl shuts treatment plants for repairs*, Retrieved September 24, 2024, 2024. [Online]. Available: https://www.asaaseradio.com/kumasi-faces-water-crisis-as-gwl-shuts-treatment-plants-for-repairs/.

[46] Pap, M. and Mahler, A., "Comparison of different empirical correlations to estimate permeability coefficient of quaternary danube soils," *Periodica Polytechnica Civil Engineering*, vol. 63, no. 1, pp. 25–29, 2019.

[47] Pitt, R. E., Clark, S., Parmer, K., and Field, R., *Groundwater Contamination from Stormwater Infiltration*, 1st. Routledge, 1996. DOI: 10.1201/9780203719756. [Online]. Available: https://doi.org/10.1201/9780203719756.

[48] Potter, E. F., Monney, I., and Rutten, M., "Bridging the data gap: using remote sensing and open-access data for assessing sustainable groundwater use in Kumasi, Ghana," *Journal of Water and Climate Change*, vol. 14, no. 9, pp. 3237–3256, Aug. 2023, ISSN: 2040-2244. DOI: 10.2166/wcc.2023.261. eprint: https://iwaponline.com/jwcc/article-pdf/14/9/3237/1301972/jwc0143237.pdf. [Online]. Available: https://doi.org/10.2166/wcc.2023.261.

[49] Rashidi Mehrabadi, M. H., Saghafian, B., and Haghighi Fashi, F., "Assessment of residential rainwater harvesting efficiency for meeting non-potable water demands in three climate conditions," *Resources, Conservation and Recycling*, vol. 73, pp. 86–93, 2013, ISSN: 0921-3449. DOI: https://doi.org/10.1016/j.resconrec.2013.01.015. [Online]. Available: https://www.sciencedirect.com/science/article/pii/S0921344913000244.

[50] Robert J. Laronga, R. L., "What makes this so different from oil and gas?" *SPE Energy Stream*, 2024. [Online]. Available: https://streaming.spe.org/webinar-seven-7-unique-appraisal-challenges-derisking-ccs-projects-or-what-makes-this-so-different-from-oil-and-gas-2.

[51] Sahajda, K., "Pile driveability prediction method based on cpt results," Jan. 2011.

[52] Skybrary, *Harmattan*, Retrieved September 15, 2024, 2024. [Online]. Available: https://skybrary.aero/articles/harmattan.

[53] Skybrary, *Monsoon*, Retrieved September 15, 2024, 2024. [Online]. Available: https://skybrary.aero/articles/monsoon.

[54] Song, S., Li, H., Yang, M., *et al.*, "Study on response process and time delay effect of groundwater dynamic in northeastern margin of tibetan plateau," *Water*, vol. 15, no. 15, p. 2838, 2023.

[55] Toure, S., Stow, D., Shih, H.-c., *et al.*, "An object-based temporal inversion approach to urban land use change analysis," *Remote Sensing Letters*, vol. 7, no. 5, pp. 503–512, 2016.

[56] Trans-African Hydro-Meteorological Observatory (TAHMO). ().

[57] TU Delft, *African water corridor*, Retrieved September 15, 2024, 2024. [Online]. Available: https://www.tudelft.nl/global/african-water-corridor.

[58] U.S. Geological Survey. "Modflow and related programs." (2024), [Online]. Available: https://www.usgs.gov/mission-areas/water-resources/science/modflow-and-related-programs (visited on 09/25/2024).

[59] United Nations Climate Action, *Water – at the center of the climate crisis*, Retrieved October 2, 2024, 2024. [Online]. Available: https://www.un.org/en/climatechange/science/climate-issues/water.

[60] United Nations Department of Economic and Social Affairs Population Division (2024). "World population prospects 2024: Data sources. (un desa/pop/2024)." (2024), [Online]. Available: https://population.un.org/wpp/ (visited on 09/15/2024).

[61] United Nations Statistics Division, *Sdg report 2022 - goal 6: Clean water and sanitation*, Retrieved October 1, 2024, 2022. [Online]. Available: https://unstats.un.org/sdgs/report/2022/Goal-06/.

[62] Van Essen Instruments. "Product manual diver®." (2016), [Online]. Available: www.vanessen.com/manuals (visited on 08/20/2024).

[63] Weather Atlas, *Kumasi, ghana - climate data*, Retrieved September 15, 2024, 2024. [Online]. Available: https://www.weather-atlas.com/en/ghana/kumasi-climate.

[64] WeatherSpark, *Average weather in kumasi, ghana: Year-round*, Retrieved September 15, 2024, 2024. [Online]. Available: https://weatherspark.com/y/40145/Average-Weather-in-Kumasi-Ghana-Year-Round#Sections-Precipitation.

[65] Webster, D., *On the edge: Shaping the future of peri-urban East Asia*. Citeseer, 2002.

[66] Wittenberg, H., Aksoy, H., and Miegel, K., "Fast response of groundwater to heavy rainfall," *Journal of Hydrology*, vol. 571, pp. 837–842, 2019.

[67] World Meteorological Organization, *City weather data*, Retrieved September 15, 2024, 2024. [Online]. Available: https://worldweather.wmo.int/en/city.html?cityId=922.

[68] World Population Review, *Kumasi, ghana - population data*, Retrieved September 15, 2024, 2024. [Online]. Available: https://worldpopulationreview.com/cities/ghana/kumasi.

[69] Yidana, S. M., Alo, C., Addai, M., Fynn, O., and Essel, S., "Numerical analysis of groundwater flow and potential in parts of a crystalline aquifer system in northern ghana," *International journal of environmental science and technology*, vol. 12, pp. 3805–3818, 2015.

[70] Yidana, S. M., Ganyaglo, S., Banoeng-Yakubo, B., and Akabzaa, T., "A conceptual framework of groundwater flow in some crystalline aquifers in southeastern ghana," *Journal of African Earth Sciences*, vol. 59, no. 2-3, pp. 185–194, 2011.

[71] Zhao, Z., Ma, Z., Huang, D., Wang, D., and Xiao, W., "A method of simulating regional groundwater level distribution based on digital elevation model," in *IOP Conference Series: Materials Science and Engineering*, IOP Publishing, vol. 392, 2018, p. 042 040.

A

Plots and Tables

A.1. Climatological Information for Kumasi

Table A.1: Climate in Kumasi, average daily minimum and maximum temperature and rainfall per month for the climatological 30-year period 1981-2010 [67].

Month	Mean daily minimum temperature (°C)	Mean daily maximum temperature (°C)	Mean total rainfall (mm)	Mean number of rain days
Jan	21.1	32.8	20.1	1.0
Feb	22.6	34.4	47.5	4.0
Mar	23.0	33.8	112.1	7.0
Apr	22.9	32.7	151.5	9.0
May	22.8	31.8	161.1	11.0
Jun	22.1	30.2	208.5	12.0
Jul	21.5	28.6	139.1	9.0
Aug	21.3	28.2	85.4	8.0
Sep	21.6	29.3	167.5	12.0
Oct	21.9	30.8	146.8	13.0
Nov	22.3	31.9	46,3	5.0
Dec	21.7	31.6	28.7	2.0

A.2. Soil Analysis

Table A.2: Values of the particles size distributions and the following hydraulic conductivity calculations of all samples.

Depth [m]	3	4	5	6	9	10	11	12	15	18	21	24	27	29	31-33
Hydraulic Conductivity [m/day]	0.80	1.95	1.35	0.79	0.63	1.90	0.58	0.93	1.48	2.37	1.64	1.62	45.72	12.01	80.11
Diameter of sieve [mm]															
75.0000	100.00	100.00	100.00	100.00	100.00	100.00	100.00	100.00	100.00	100.00	100.00	100.00	100.00	100.00	100.00
63.0000	100.00	100.00	100.00	100.00	100.00	100.00	100.00	100.00	100.00	100.00	100.00	100.00	100.00	100.00	100.00
53.0000	100.00	100.00	100.00	100.00	100.00	100.00	100.00	100.00	100.00	100.00	100.00	100.00	100.00	100.00	100.00
37.1000	100.00	100.00	100.00	100.00	100.00	100.00	100.00	100.00	100.00	100.00	100.00	100.00	100.00	100.00	100.00
25.4000	100.00	100.00	100.00	100.00	100.00	100.00	100.00	100.00	100.00	100.00	100.00	100.00	100.00	100.00	100.00
19.0000	100.00	100.00	100.00	100.00	100.00	100.00	100.00	100.00	100.00	100.00	100.00	100.00	100.00	100.00	100.00
13.2000	100.00	100.00	100.00	100.00	100.00	100.00	100.00	100.00	100.00	100.00	100.00	100.00	100.00	100.00	100.00
9.5000	100.00	100.00	100.00	100.00	100.00	100.00	100.00	100.00	100.00	100.00	100.00	100.00	100.00	100.00	100.00
6.7000	100.00	100.00	100.00	100.00	100.00	100.00	100.00	100.00	100.00	97.82	100.00	100.00	100.00	100.00	100.00
4.7500	100.00	100.00	100.00	100.00	100.00	100.00	100.00	100.00	100.00	97.82	100.00	100.00	100.00	100.00	100.00
3.3500	99.52	99.46	99.50	99.62	99.61	98.95	99.38	99.42	99.34	96.70	99.90	99.86	100.00	100.00	100.00
2.0000	94.84	94.75	97.32	97.17	95.57	93.60	95.76	95.10	96.84	93.05	98.39	97.82	97.67	97.58	100.00
1.0000	80.23	77.23	80.72	82.93	82.23	78.72	81.26	80.02	83.52	80.64	87.39	85.71	73.52	79.76	71.19
0.6000	71.39	66.09	67.35	71.94	73.44	70.39	70.88	70.24	72.76	69.35	75.99	74.39	42.28	58.60	31.25
0.4250	67.41	61.44	62.00	66.91	69.24	65.95	66.39	65.45	67.31	63.29	69.36	67.93	28.37	46.97	20.41
0.3000	64.19	57.96	58.16	62.93	65.56	62.19	62.60	61.39	61.89	57.71	62.82	62.02	20.35	37.70	15.00
0.1500	59.02	53.37	53.79	57.41	59.09	57.45	56.82	54.04	51.43	47.84	51.32	51.40	14.29	27.50	10.83
0.0750	53.88	49.54	50.99	53.41	52.60	53.68	51.39	46.46	41.80	39.59	41.98	43.54	11.87	22.79	9.20
0.0669	25.091	21.778	21.810	28.803	27.244	25.382	22.645	22.141	17.195	13.692	17.161	15.100	0.452	2.717	0.646
0.0479	23.516	19.563	20.983	26.205	23.768	23.825	21.752	18.369	15.838	12.406	15.122	12.978	0.260	2.347	0.557
0.0346	20.890	18.759	20.155	23.953	20.291	22.269	19.072	16.106	14.482	11.121	13.083	10.856	0.183	1.977	0.497
0.0247	19.840	17.956	19.327	21.700	17.684	21.923	16.392	14.597	12.447	9.192	10.637	6.865	0.067	1.238	0.438
0.0183	13.889	17.474	19.327	19.102	13.650	21.750	12.819	11.433	10.412	7.521	9.685	6.158	-0.125	1.090	0.379
0.0134	11.683	17.153	18.996	16.849	11.390	20.675	11.389	9.316	7.632	5.978	7.375	5.026	-0.172	1.001	0.275
0.0098	7.970	15.546	18.003	14.944	7.914	19.983	8.352	5.471	6.275	4.790	5.608	5.026	-0.249	0.409	0.186
0.0071	5.787	15.224	17.009	12.865	6.039	19.119	5.672	5.507	4.783	3.633	3.977	2.197	-0.441	0.039	0.200
0.0051	4.036	14.182	16.182	11.563	4.301	18.463	3.349	5.242	3.493	2.733	3.466	0.783	-0.510	-0.241	0.126
0.0037	2.268	13.258	15.428	9.885	2.293	17.849	1.999	2.574	2.314	1.550	2.319	0.008	-0.691	-0.957	0.002
0.0015	0.360	11.579	12.757	7.287	-0.511	15.923	-1.419	0.311	0.897	0.710	0.899	-1.406	-0.733	-1.038	-0.011

A.3. Timeseries of five minute data from pilot wells

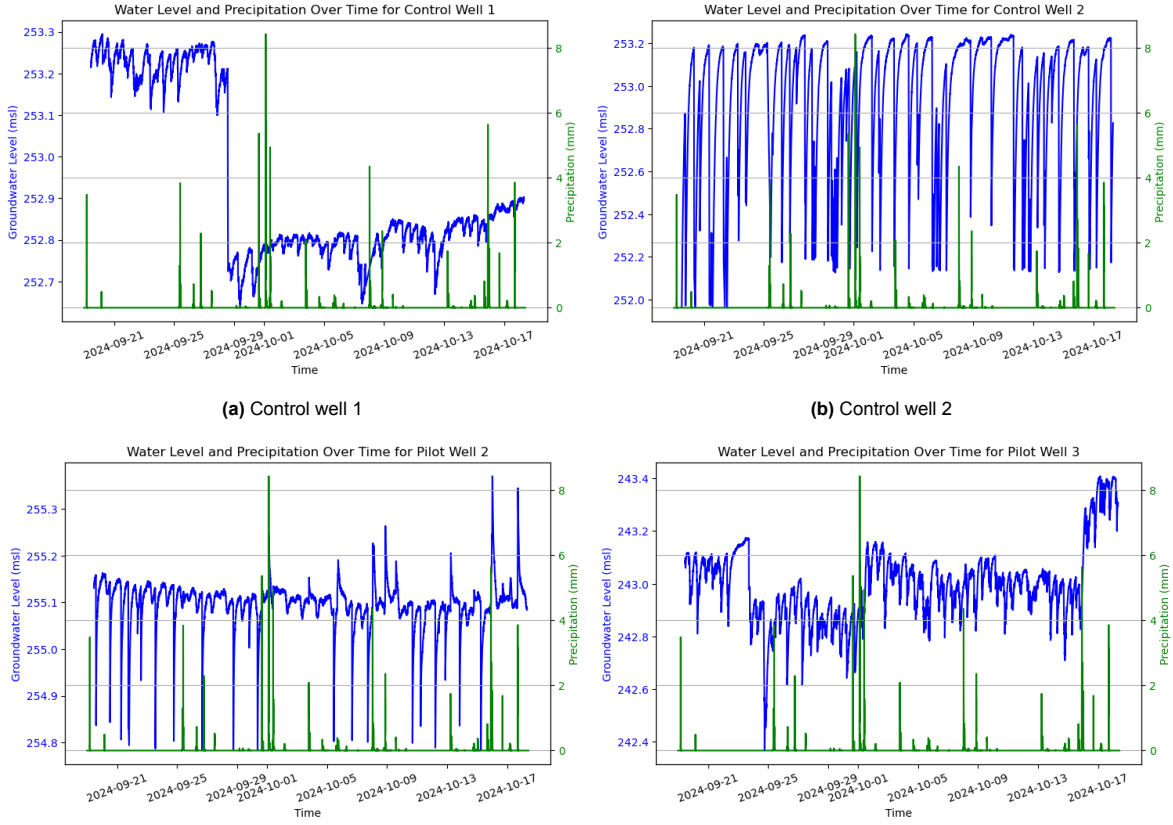

(a) Control well 1

(b) Control well 2

(c) Pilot well 2

(d) Pilot well 3

Figure A.1: Time series of the groundwater level (green) and precipitation (blue), both collected every five minutes, from 19-09-2024 to 17-10-024 for all wells at the pilot site, except for pilot well 1 (no data available) and pilot well 4 (presented in the results). Note that the axes of the groundwater levels are different.

A.4. Correlation between daily water level and precipitation

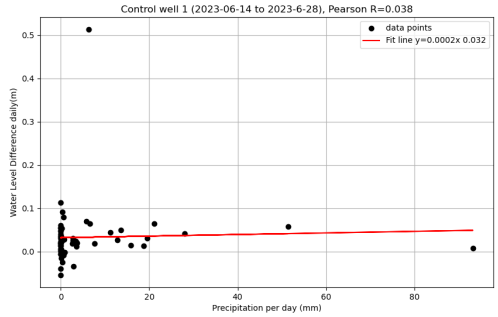

(a) Control well 1

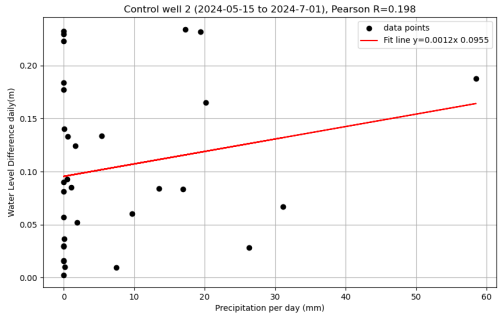

(b) Control well 2

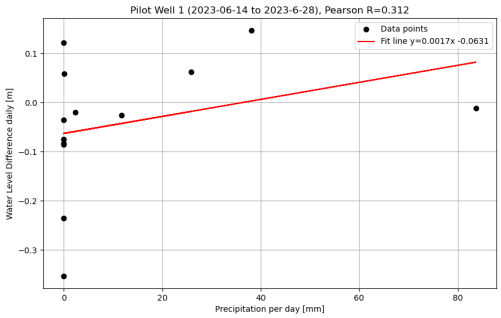

(c) Pilot well 1

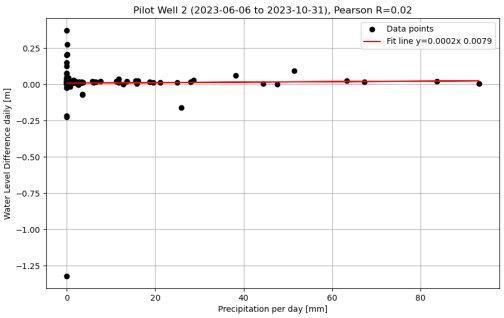

(d) Pilot well 2

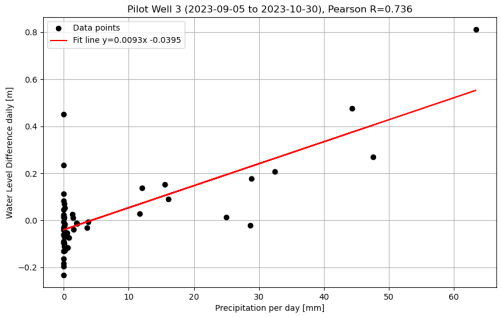

(e) Pilot well 3

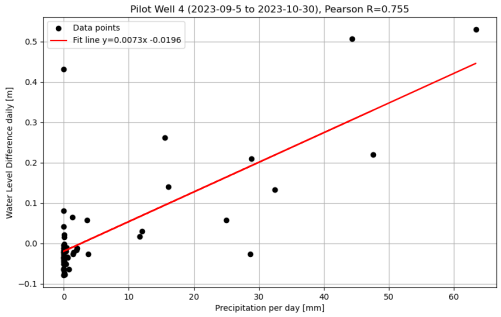

(f) Pilot well 4

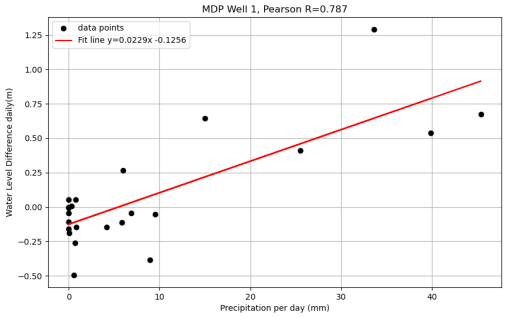

(g) MDP well 1

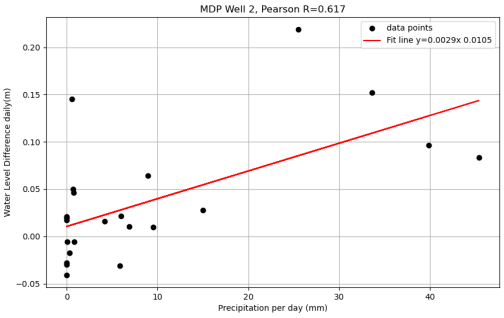

(h) MDP well 2

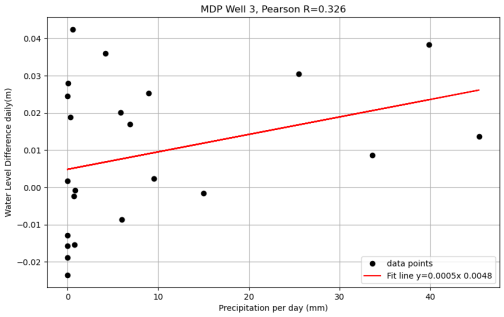

(i) MDP well 3

Figure A.2: Correlation of daily groundwater level difference of each well and the daily precipitation from TAHMO based on Chyan-Deng Jan et. al. (2007)

A.5. MODFLOW 6 Models

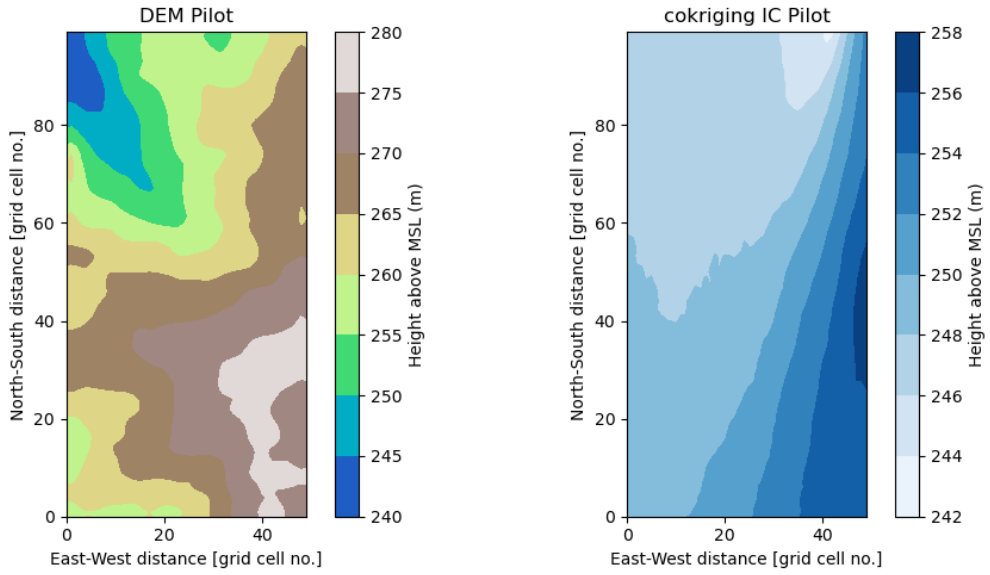

Figure A.3: Digital Elevation Map (left) and map of the initial hydraulic heads found by cokriging (right) for the pilot site.

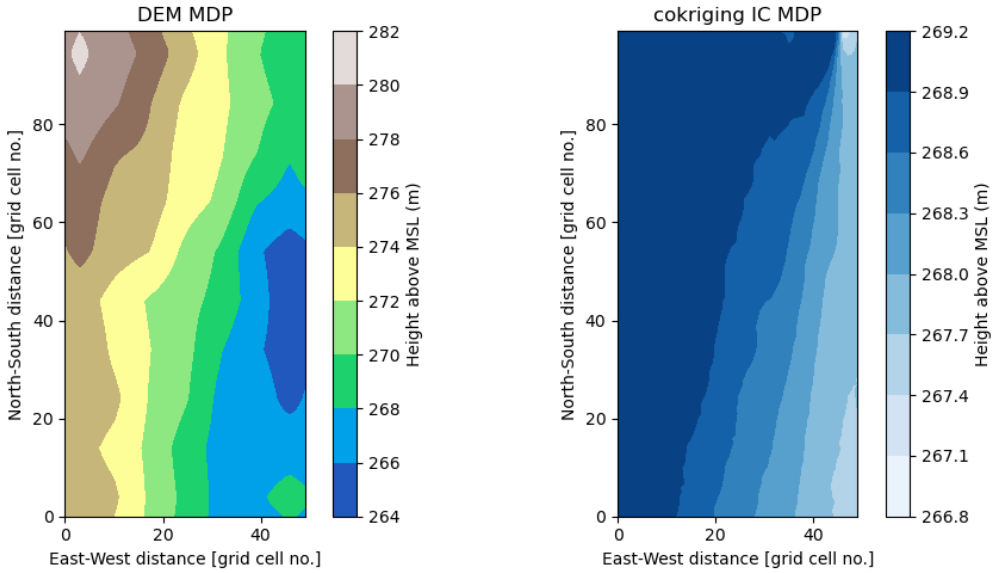

Figure A.4: Digital Elevation Map (left) and map of the initial hydraulic heads found by co-kriging (right) for the mdp site.

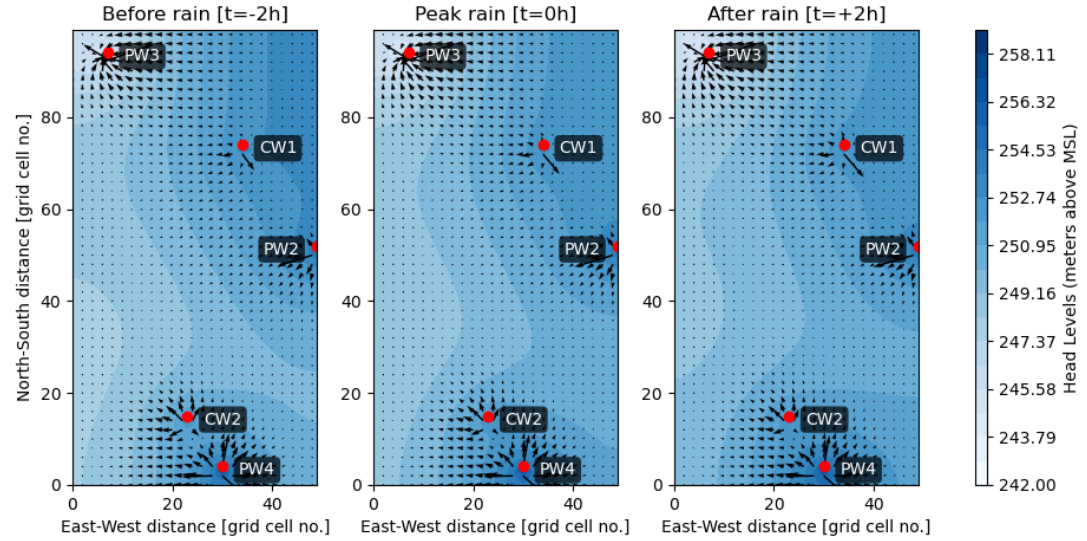

Figure A.5: Pilot site top view of the bottom layer before, during and after a singular rain event. The flow still follows the elevation, though less than in the top layer.

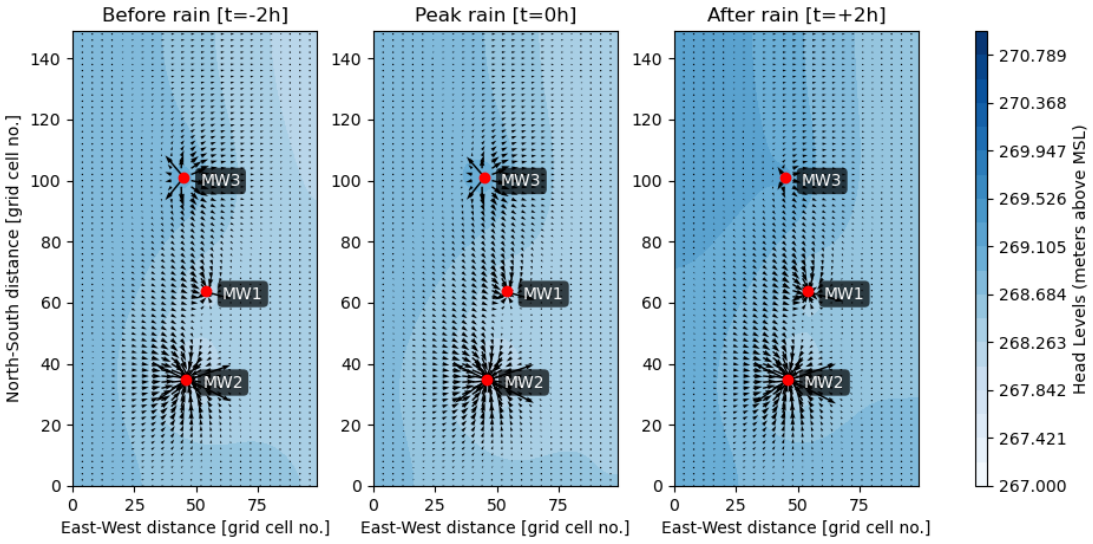

Figure A.6: MDP site top view of the bottom layer before, during, and after a singular rain event. The flow does not follow the elevation, but rather the changes in hydraulic head only. The response is significantly less than the upper layer.

B

Task Division

Table B.1: Distribution of the workload

	Task	Student Name(s)
Processing	Correlations	Evangelos, Lilian
	Precipitation	Irene
	Diver data	Evangelos, Lilian, Irene
	Soil data	Tara, Zeyu
	Soil data, lab	All
	MODFLOW 6 models	Tara, Irene
	2D simulator	Zeyu
Writing	Acknowledgements	Tara
	Summary	Tara
	Introduction	Lilian
	Background	Irene, Tara
	Methodology	Evangelos, Lilian, Zeyu
	Results	Lilian, Tara, Irene
	Experimental Trial of 2D Simulator	Zeyu
	Discussion	Zeyu, Evangelos, Lilian
	Conclusion	Zeyu, Evangelos
	Recommendations	Irene
Reviewing		All